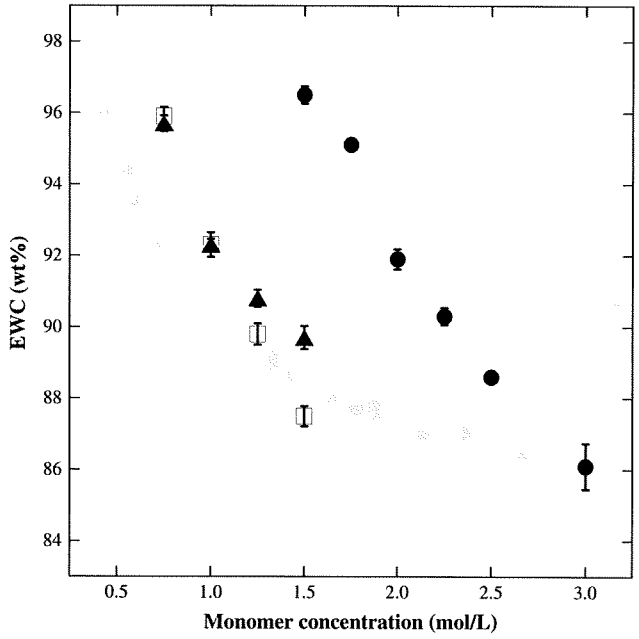


**Fig. 2.** EWC of the three types of hydrogels at the concentrations of the monomer solutions: poly(MPC) (●), poly(Me(EG)$_4$MA) (□), and poly(Me(EG)$_8$MA) (▲) hydrogels. The plotted values are the average of six measurements, and double the standard deviation is used as the range of errors in the values.

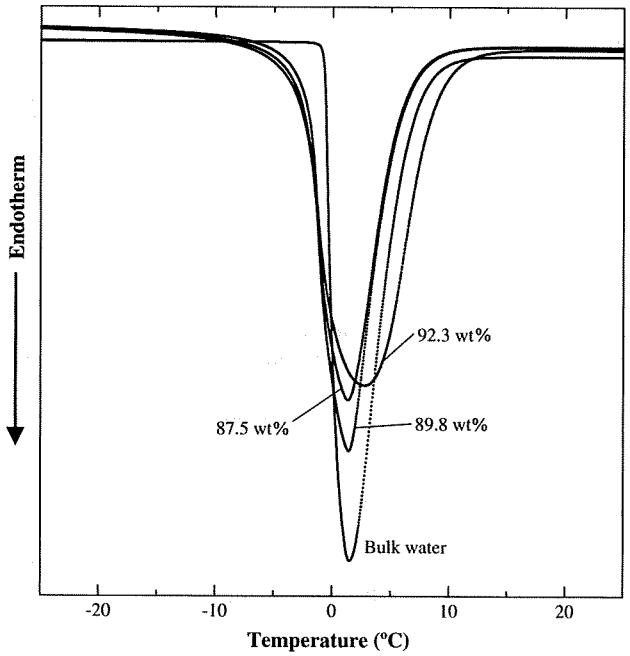


**Fig. 4.** DSC thermograms at a heating rate of 5 °C/min for the poly(Me(EG)$_4$MA) hydrogels with different EWCs and for bulk water. The values indicated in the figure show the EWCs.

could not observe any enthalpy change for freeze-dried poly(MPC) hydrogels in the temperature range, indicating that the polymer chains have no contribution to the endothermic behavior. Herein, it was concluded that the peak was derived from the melting of freezable water in the poly(MPC) hydrogels. As with the poly(MPC) hydrogels, the thermograms of the poly(Me(EG)$_4$MA) and poly(Me(EG)$_8$MA) hydrogels yielded single endothermic peak due to the melting of freezable water. In all the hydrogels, no other thermal transitions were observed during the heating experiments.

In accordance with the earlier studies on hydrated polymer materials [17,26], the single endothermic peak observed for each hydrogel was broad toward the low-temperature side, which was in contrast to that for bulk water. This results from the distribution of the melting temperature of freezable water in the hydrogels [27].

From the area of each single peak, we estimated the enthalpy change ($\Delta H_f$) associated with the melting of freezable water in the hydrogels. The values of $\Delta H_f$ for the poly(MPC), poly(Me(EG)$_4$MA), and poly(Me(EG)$_8$MA) hydrogels are plotted as a function of EWC in

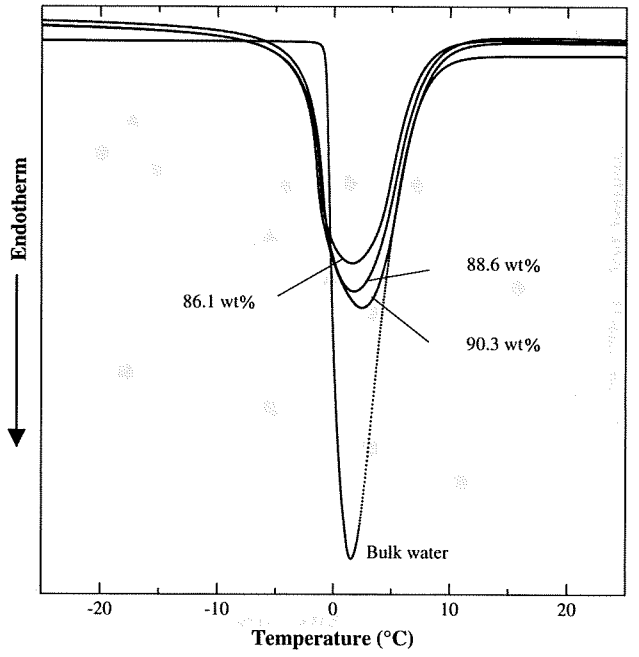


**Fig. 3.** DSC thermograms at a heating rate of 5 °C/min for the poly(MPC) hydrogels with different EWCs and for bulk water. The values indicated in the figure show the EWCs.

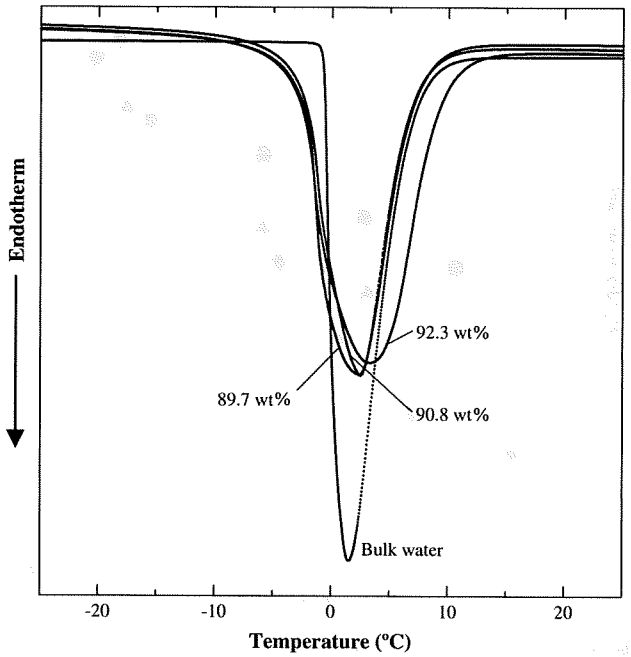


**Fig. 5.** DSC thermograms at a heating rate of 5 °C/min for the poly(Me(EG)$_8$MA) hydrogels with different EWCs and for bulk water. The values indicated in the figure show the EWCs.

Fig. 6. The values were less than those estimated on the supposition that all the water contained in the hydrogels behave as freezable water, which indicated that a certain amount of water in the hydrogels was unable to freeze. From the $\Delta H_f$ values, the amounts of freezable and nonfreezable water in the hydrogels can be calculated. The weight ($W_{freezable}$) of freezable water relative to that of the polymer in a hydrogel is expressed by

$$W_{freezable} = \frac{w_{freezable}}{w_{polymer}} \quad (2)$$

where $w_{freezable}$ and $w_{polymer}$ are the weight percents of freezable water and polymer in the hydrogel, respectively. Since the weight percent ($w_{nonfreezable}$) of nonfreezable water in a hydrogel is the difference between the total water content, namely EWC, and $w_{freezable}$, the weight ($W_{nonfreezable}$) of nonfreezable water relative to that of the polymer in a hydrogel is given by

$$W_{nonfreezable} = \frac{w_{nonfreezable}}{w_{polymer}} = \frac{EWC - w_{freezable}}{w_{polymer}} \quad (3)$$

Here, $w_{freezable}$ can be experimentally obtained by using $\Delta H_f$ and can be expressed by the following equation:

$$w_{freezable} = \frac{\Delta H_f}{\Delta H_w} \times 100 \quad (4)$$

where $\Delta H_f$ is the enthalpy change associated with the melting of freezable water per weight of a hydrogel and $\Delta H_w$ is the enthalpy change for the melting of bulk water. On the basis of Eq. (4), Eqs. (2) and (3) can be rewritten as

$$W_{freezable} = \frac{1}{w_{polymer}}\left(\frac{\Delta H_f}{\Delta H_w} \times 100\right) \quad (5)$$

$$W_{nonfreezable} = \frac{1}{w_{polymer}}\left(EWC - \frac{\Delta H_f}{\Delta H_w} \times 100\right) \quad (6)$$

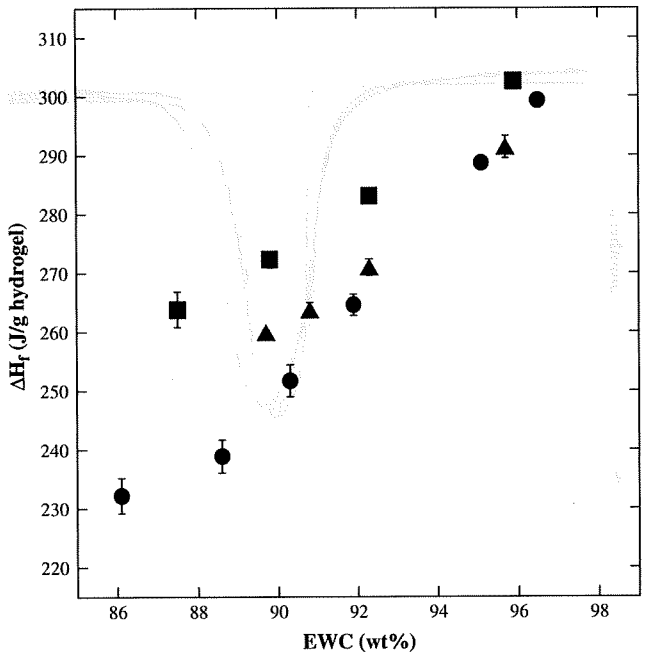


**Fig. 6.** Enthalpy changes associated with the melting of freezable water in the hydrogels as a function of EWC: poly(MPC) (●), poly(Me(EG)$_4$MA) (■), and poly(Me(EG)$_8$MA) (▲) hydrogels. The plotted values are relative to the weight of each hydrogel and were the average of four measurements. The standard deviation is used as the range of errors in the values.

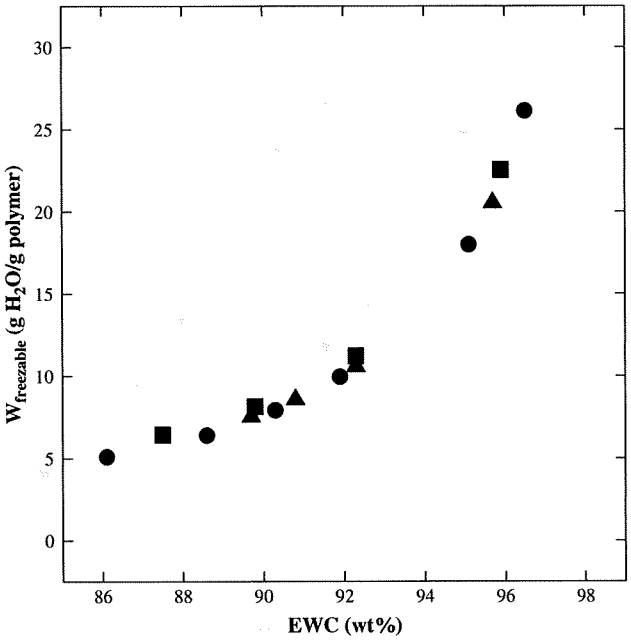


**Fig. 7.** Weight of freezable water relative to that of the polymer in the hydrogels as a function of EWC: poly(MPC) (●), poly(Me(EG)$_4$MA) (■), and poly(Me(EG)$_8$MA) (▲) hydrogels. The plotted values are the average of four measurements, and the standard deviation is used as the range of errors in the values.

$\Delta H_w$ measured for the distilled water used in this study was 327.5 ± 1.4 J/g (mean ± S.D., $n = 4$), which is almost the same value of bulk water (333.5 J/g). The measured $\Delta H_w$ value was used in Eqs. (5) and (6).

The $W_{freezable}$ and $W_{nonfreezable}$ values for the poly(MPC), poly(Me(EG)$_4$MA), and poly(Me(EG)$_8$MA) hydrogels are plotted as a function of EWC in Figs. 7 and 8, respectively. In Fig. 7, no significant differences were observed in the comparison of the $W_{freezable}$ values for the given values of EWC between the three

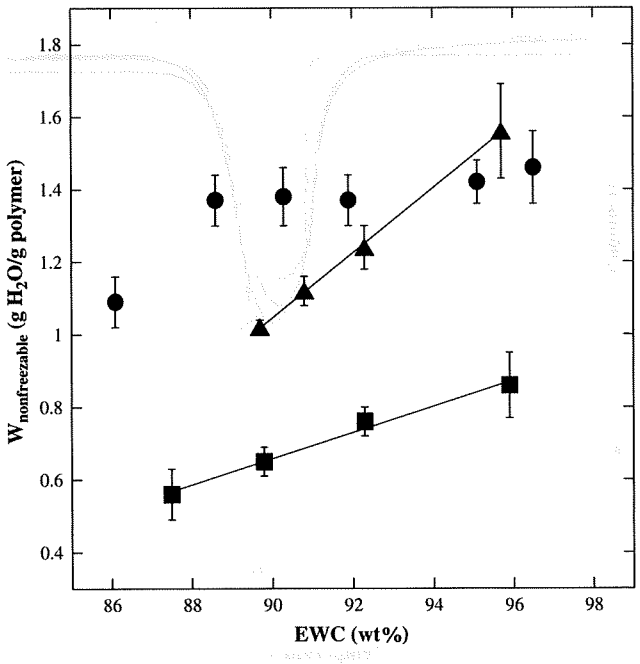


**Fig. 8.** Weight of nonfreezable water relative to that of the polymer in the hydrogels as a function of EWC: poly(MPC) (●), poly(Me(EG)$_4$MA) (■), and poly(Me(EG)$_8$MA) (▲) hydrogels. The plotted values are the average of four measurements, and the standard deviation is used as the range of errors in the values.

types of hydrogels. However, this result does not indicate that the amount of freezable water in the three types of hydrogels depends on the EWC. As seen in Fig. 6, the $\Delta H_f$ values for the given values of EWC differed between the hydrogels, especially in the EWC range from 86 to 92 wt%. According to Eq. (4), this difference remarkably influences the $w_{freezable}$ values. Among the hydrogels, the $w_{freezable}$ values for the given values of EWC clearly decreased in the order corresponding to poly(Me(EG)$_4$MA), poly(Me(EG)$_8$MA), and poly(MPC) hydrogels. By transforming the $w_{freezable}$ values into $W_{freezable}$ values using Eq. (5), little differences in the $W_{freezable}$ values among the hydrogels with similar EWC could be seen.

In contrast, the $W_{nonfreezable}$ values showed the large differences between the hydrogels. As shown in Fig. 8, the $W_{nonfreezable}$ values for the poly(MPC) hydrogels increased from 1.09 to 1.37 g $H_2O$/g polymer when the EWC was increased from 86.1 to 88.6 wt%. Moreover, the values did not change significantly (1.37–1.46 g $H_2O$/g polymer) with the increase in the EWC. On the other hand, the $W_{nonfreezable}$ values for the poly(Me(EG)$_4$MA) and poly(Me(EG)$_8$MA) hydrogels linearly increased with the EWC. For the poly(Me(EG)$_4$MA) hydrogels, the $W_{nonfreezable}$ values changed from 0.56 to 0.86 g $H_2O$/g polymer, whereas the changes in the $W_{nonfreezable}$ values for the poly(Me(EG)$_8$MA) hydrogels were from 1.02 to 1.56 g $H_2O$/g polymer. The poly(MPC) hydrogels showed higher $W_{nonfreezable}$ values as compared with the poly(Me(EG)$_4$MA) and poly(Me(EG)$_8$MA) hydrogels, except for the values comparable with the poly(Me(EG)$_8$MA) hydrogels when the EWC was above 95 wt%. This shows the higher hydrating ability of the poly(MPC) chains than that of the poly(Me(EG)$_4$MA) and poly(Me(EG)$_8$MA) chains. In addition, the $W_{nonfreezable}$ values for the poly(MPC) hydrogels were higher than those for protein- or polysaccharide-based materials, which have often been used as biomaterials, for similar total water contents [28–30]. It should be noted that the $W_{nonfreezable}$ values for the poly(MPC) hydrogels were constant with regard to the EWC, while those for the poly(Me(EG)$_4$MA) and poly(Me(EG)$_8$MA) hydrogels linearly increased with the EWC. We think that this feature may be related to the overlap of the hydration shells of polymer chains. In general, as the EWC of polymer hydrogels is decreased, the entanglement of polymer chains is enhanced. This leads to a decrease in the space among polymer chains. Here, the hydration shells of polymer chains overlap when the chains are mutually at some distance [31]. The constant $W_{nonfreezable}$ values for the poly(MPC) hydrogels might be caused by the absence of the overlap of the hydration shells.

Finally, we discussed the origin of nonfreezable water around poly(MPC) chains. The $W_{nonfreezable}$ values for poly(MPC) chains were transformed into the number ($N_w$) of nonfreezable water molecules per poly(MPC) repeating unit by the following equation:

$$N_w = W_{nonfreezable} \times \frac{M_p}{M_w} \quad (7)$$

where $M_p$ is the molecular weight per polymer repeating unit ($M_p = 295$ for poly(MPC)) and $M_w$ is the molecular weight of water. The results are summarized in Table 1. The $N_w$ value per poly(MPC) repeating unit was 23–24. The phosphorylcholine groups in poly(MPC) chains are bulky and hydrophilic, so they have the large hydration capacity. Also, the value was consistent with the number of water molecules associated with each phosphorylcholine group in dodecylphosphorylcholine surfactants below the critical micelle concentration, that is, 24–25 [32]. As represented by the interaction with PEG chains of water, the formation of nonfreezable water in polymer–water systems has frequently been explained as a result of the hydrogen bonds between water molecules and polymer chains [17,26,28]. However, poly(MPC) chains have difficulty in the formation of the 23–24 nonfreezable water molecules by only the hydrogen bonds with water molecules because the primary atoms that can form hydrogen bonds with water molecules are one carbonyl oxygen and two non-ester phosphate oxygens per repeating unit. A possible explanation for the origin of nonfreezable water molecules around poly(MPC) chains may be the weak electrostatic interaction of water molecules with zwitterionic groups in phosphorylcholine groups. Kitano et al. showed that poly(MPC) chains did not significantly disturb the hydrogen bonds between their surrounding water molecules, suggesting that the phosphorylcholine groups may counteract the electrostatic hydration [33,34]. It is clear that further study is needed to characterize the origin of the nonfreezable water molecules. We believe that it can be achieved by NMR relaxation time measurements or vibrational spectroscopy such as infrared and Raman, since these methods can probe the faster motion of water networks than thermal analysis and especially, vibrational spectroscopy can provide information on local water networks.

**Table 1**
Number ($N_w$) of nonfreezable water molecules per poly(MPC) repeating unit

| EWC (wt%) | 96.5 | 95.1 | 91.9 | 90.3 | 88.6 | 86.1 |
|---|---|---|---|---|---|---|
| $N_w$[a] | 24 ± 2 | 23 ± 1 | 23 ± 1 | 23 ± 1 | 23 ± 1 | 18 ± 1 |

[a] The values were obtained by averaging the results of four measurements, and the standard deviation was used as the range of errors in these values.

## 4. Conclusion

Hydration of poly(MPC) chains was investigated by using chemically cross-linked poly(MPC) hydrogels in the EWC range from 86.1 to 96.5 wt%. It was compared with that of poly(Me(EG)$_4$MA) and poly(Me(EG)$_8$MA) chains with a similar hydration level. From the results of the enthalpy change associated with the ice-to-water transitions in the hydrogels obtained by DSC measurements, poly(MPC) chains had a higher amount of nonfreezable water than poly(Me(EG)$_4$MA) and poly(Me(EG)$_8$MA) chains. The high hydrating ability of poly(MPC) chains was kept at a high level in the EWC range. In addition, it was suggested that nonfreezable water around poly(MPC) chains was derived from electrostatic interaction as well as hydrogen bonds. It has been observed that poly(MPC) chains resist platelet adhesion and protein denaturalization for longer periods than OEG-monomethacrylate polymer and PEG chains. Thus, the results in this study may indicate that the nonfreezable water around polymer chains detected by thermal analysis may be one of the promising parameters for considering a longer duration of resistance against the protein adsorption. This study is our starting point for the establishment of hydration parameters that can characterize the relationship between the outcome of protein adsorption resistance and hydration of materials.

## Acknowledgement

A part of this research was supported by the Core Research for Evolution Science and Technology (CREST) from Japan Science and Technology Agency.

## References

[1] Ratner BD, Hoffman FJ, Schoen JE, Lemos F. Biomaterials science. An introduction to materials in medicine. New York: Academic Press; 1996.
[2] Chen CS, Mrksich M, Huang S, Whitesides GM, Ingber DE. Science 1997;276:1425–8.
[3] Santini JT, Cima MJ, Langer R. Nature 1999;397:335–8.
[4] Park J, Kurosawa S, Watanabe J, Ishihara K. Anal Chem 2004;76:2649–55.
[5] Brash JL. J Biomater Sci Polym Ed 2000;11:1135–46.
[6] Kenausis GL, Vörös J, Elbert DL, Huang N, Hofer R, Ruiz-Taylor L, et al. J Phys Chem B 2000;104:3298–309.
[7] Chen S, Zheng J, Li L, Jiang S. J Am Chem Soc 2005;127:14473–8.
[8] Feng W, Zhu S, Ishihara K, Brash JL. Biointerphases 2006;1:50–60.
[9] Sigal GB, Mrksich M, Whitesides GM. J Am Chem Soc 1998;120:3464–73.
[10] Vogler EA. Adv Colloid Interface Sci 1998;74:69–117.

[11] Ostuni E, Chapman RG, Holmin RE, Takayama S, Whitesides GM. Langmuir 2001;17:5605–20.
[12] Nagaoka S, Mori Y, Takiuchi H, Yokota K, Tanzawa H, Nishiumi S. Interaction between blood components and hydrogels with poly(oxyethylene) chains. In: Shalaby SW, editor. Polymers as biomaterials. New York: Plenum Press; 1984. p. 361–74.
[13] Jeon SI, Lee JH, Andrade JD, de Gennes PG. J Colloid Interface Sci 1991; 142:149–58.
[14] Prime KL, Whitesides GM. J Am Chem Soc 1993;115:10714–21.
[15] Holmin RE, Chen X, Chapman RG, Takayama S, Whitesides GM. Langmuir 2001;17:2841–50.
[16] Morra M. Water in biomaterials surface science. Chichester: John Wiley & Sons; 2001.
[17] Antonsen KP, Hoffman AS. Water structure of PEG solutions by differential scanning calorimetry measurement. In: Harris JM, editor. Poly(ethylene glycol) chemistry: biotechnical and biomedical applications. New York: Plenum Press; 1992. p. 15–28.
[18] Wang RLC, Kreuzer HJ, Grunze M. J Phys Chem B 1997;101:9767–73.
[19] Wang RY, Himmelhaus M, Fick J, Herrwerth S, Eck W, Grunze M. J Chem Phys 2005;122:164702–6.
[20] Ishihara K, Ueda T, Nakabayashi N. Polym J 1990;22:355–60.
[21] Iwasaki Y, Ishihara K. Anal Bioanal Chem 2005;381:534–46.
[22] Watanabe J, Ishihara K. Colloids Surf B 2008;65:155–65.
[23] Ishihara K, Iwasaki Y, Ebihara S, Shindo Y, Nakabayashi N. Colloids Surf B 2000;18:325–35.
[24] Ishihara K. The role of water in the surface properties of phospholipid polymers. In: Morra M, editor. Water in biomaterials surface science. Chichester: John Wiley & Sons; 2001. p. 333–51.
[25] Kiritoshi Y, Ishihara K. J Biomater Sci Polym Ed 2002;13:213–24.
[26] Huang L, Nishinari K. J Polym Sci Part B Polym Phys 2001;39:496–506.
[27] Kuntz ID, Kauzmann W. Adv Protein Chem 1974;28:239–345.
[28] Joshi HN, Topp EM. Int J Pharm 1992;80:213–25.
[29] Liu WG, Yao KD. Polymer 2001;42:3943–7.
[30] Megeed Z, Cappello J, Ghandehari H. Biomacromolecules 2004;5:793–7.
[31] Kjellander R, Florin E. J Chem Soc Faraday Trans 1 1981;77:2053–77.
[32] Yaseen M, Lu JR, Webster JRP, Penfold J. Langmuir 2006;22:5825–32.
[33] Kitano H, Sudo K, Ichikawa K, Ide M, Ishihara K. J Phys Chem B 2000;104:11425–9.
[34] Kitano H, Imai M, Mori T, Gemmei-Ide M, Yokoyama Y, Ishihara K. Langmuir 2003;19:10260–6.

FULL PAPER *Surgery*

# Prevention of Biofilm Formation with a Coating of 2-Methacryloyloxyethyl Phosphorylcholine Polymer

Kiyohisa FUJII[1], Hiroko N. MATSUMOTO[1], Yoshihisa KOYAMA[1], Yasuhiko IWASAKI[1], Kazuhiko ISHIHARA[2] and Kazuo TAKAKUDA[1]*

[1]*Institute of Biomaterials and Bioengineering, Tokyo Medical and Dental University, 2–3–10 Kanda-Surugadai, Chiyoda-ku, Tokyo 101–0062 and* [2]*Department of Materials Engineering, School of Engineering, The University of Tokyo, 7–3–1 Hongou, Bunkyou-ku, Tokyo 113–8656, Japan*

(Received 27 June 2007/Accepted 19 October 2007)

ABSTRACT. Device-associated infections are serious complications, and their prevention is an issue of considerable importance. Since biofilms are responsible for these refractory infections, effective methods to inhibit biofilm formation are required. In this investigation, stainless steel plates with and without 2-methacryloyloxyethyl phosphorylcholine (MPC) polymer, i.e., poly (MPC-co-n-butyl methacrylate) (PMB) coating, were incubated in a medium containing bacteria. In the course of incubation, half of the specimens received antibiotics. The specimens were stained for nucleic acid and polysaccharides, and then examined with a confocal laser scanning microscope. The numbers of bacteria on the specimen surfaces were evaluated by an ATP assay. On the surfaces of the specimens without PMB coating, the formation of a biofilm enveloping bacteria was confirmed. The addition of antibiotics did not effectively decrease the number of bacteria. On the other hand, on the surfaces of the specimens with PMB coating, no biofilm formation was observed, and the number of bacteria was significantly decreased. The addition of potent antibiotics further decreased the number of bacteria by 1/100 to 1/1000 times. The PMB coating combined with the validated use of antibiotics might provide a method for the simultaneous achievement of biocompatible surfaces of devices and the prevention of device-associated infections.

KEY WORDS: biofilm, biomaterials, device-associated infection, MPC, PMB coating.

*J. Vet. Med. Sci.* 70(2): 167–173, 2008

Device-associated infections are serious complications in patients receiving indwelling catheters. These complications, however, do not limited in such cases; device-associated infections are consistent risk accompanying the usage of any artificial devices. For instance, applications of bone fixation plates to open fractures are contraindicated. Actually, the rate of the infections was reported to be as high as 15% to 18% [23] if an aseptic condition was not maintained during the treatment. Although the microorganisms responsible for these infections are usually indigenous bacteria such as *Staphylococcus epidermidis*, a difficulty arises as antibacterial agents are not effective against these infections. Once the infections are established, persistent inflammations continue as long as the devices remain in the body.

Device-associated infections are caused by bacteria that adhere to the surfaces of internal prosthetic devices and are thought to develop through the following sequence of events [3, 7, 10, 18, 22]. Immediately after the implantation of devices into patients, various molecules such as peptides and proteins are adsorbed onto the surfaces of the materials. These molecules mediate the attachment of bacteria. Once the bacteria, e.g., those belonging to the species *S. epidermidis*, are attached to the surfaces of devices, they proliferate and aggregate there to form biofilms in which the bacteria are enveloped in a thin layer of polysaccharides. The bacteria in the biofilms are protected from the biological defense mechanism, including phagocytosis by macrophages and immunological responses, as well as antibacterial agents for therapeutic use. Hence, the formation of biofilms on the surface of devices establishes refractory infections, i.e., device-associated infections [6, 8, 19, 24, 27, 28].

Various strategies were proposed and are expected to be effective in preventing device-associated infections. Wassall [31] utilized silver coating on stainless steel pins for external skeletal fixation and reported successful infection control. Takahashi [29] developed antibacterial catheters coated with citrate silver and lecithin and reported that biofilm formations were prevented. In these reports, silver coating that has an antibacterial effect was utilized; however, silver is not a biocompatible material and might exert adverse effects on living tissues. It is desirable to realize another approach in which only biocompatible materials are utilized for preventing device-associated infections.

2-Methacryloyloxyethyl phosphorylcholine (MPC) was designed taking into account the surface structure of the biomembrane. MPC polymers have a surface that resists nonspecific protein adsorption and cell adhesion [13–17, 25]. It has been attracting considerable attention for its remarkable antithrombogenicity and has been applied successfully to artificial blood vessels, implantable artificial hearts and artificial lungs. The MPC polymer coating renders the surfaces extremely hydrophilic, prevents the adhesion of proteins, and inhibits the adhesion of platelets. Noting the similarity of platelet adhesion and bacterial adhesions, we might expect that the MPC polymer coating also leads to the inhibition of bacterial adhesion and the forma-

* CORRESPONDENCE TO: TAKAKUDA, K.., Institute of Biomaterials and Bioengineering, Tokyo Medical and Dental University, 2–3–10 Kanda-Surugadai, Chiyoda-ku, Tokyo 101–0062, Japan.
e-mail: takakuda.mech@tmd.ac.jp

tion of biofilm. In fact, Hirota *et al.* [9] had coated coverslips made of polyethylenetelephthalate with MPC polymer and observed decreased adhesion of bacteria to the coverslip surfaces. In their experiments, however, they exposed the specimens to bacteria for only 1 hr and counted the number of bacteria attached to the specimens during this period. In order to elucidate whether MPC polymer coating prevents biofilm formation, a comparative study concerning biofilm formation on noncoated and MPC polymer-coated surfaces, which requires a longer period of exposure to bacteria, should be conducted. Hence, in this investigation, we carried out biofilm formation experiments with both surfaces and examined how MPC polymer, i.e., poly[MPC-co-n-butyl methacrylate (BMA)] (PMB) coating inhibits the formation of biofilms.

## MATERIALS AND METHODS

*Plate specimens*: Stainless steel plates (SUS316L; Nilaco Corp., Tokyo, Japan) with a thickness of 0.1 mm and dimensions of 5 × 5 × 0.1 mm were prepared. The composition of this material was standardized for medical use such as bone fixation devices. Since surface characteristics as bacterial adhesion were examined in this experiment, thin plates of 0.1-mm thickness were adopted for the sake of convenience in cultivation. The specimens were cleaned with acetone, washed with distilled water, and autoclaved at 121°C for 20 min. Further operations with the specimens were carried out in sterile conditions.

*Coating with MPC polymer*: The MPC was synthesized as previously reported [14]. The PMB was synthesized by radical polymerization of desired amount of MPC and n-butyl methacrylate in ethanol using 2,2'-azobisisobutyronitrile (AIBN) as an initiator [16]. The chemical structure of the PMB was determined by $^1$H-NMR and IR spectroscopies. The composition of the MPC unit was 30 mol%. The structural formula of PMB [12] is illustrated in Fig. 1. The PMB was resolved in ethanol, and the concentration was adjusted to 0.5% (wt/vol). The stainless steel specimens were immersed in the PMB solution and then dried on a clean bench. Before the specimens thus coated with PMB were used in culture experiments, they were immersed in calcium- and magnesium-free phosphate-buffered saline (PBS(–), pH 7.2) ) for 30 min.

*Bacterial preparation*: *Staphylococcus aureus* (JCM 2151), *S. epidermidis* (JCM 2414), and *Pseudomonas aeruginosa* (JCM 2412) were purchased from Japan Collection of Microorganisms (Riken BioResource Center, Wako, Japan) and utilized in this investigation.

*Cultivation experiments for confocal laser scanning microscope (CLSM) observation*: Organisms were grown in the culture medium reported by Akiyama *et al.* [1], that was soybean-casein digest broth (Nihon Pharm., Tokyo, Japan) supplemented with the same amount of normal rabbit plasma (Denka Seiken, Tokyo, Japan). Cultivation experiments were performed following the previous reports [1, 9, 11, 27, 30]. Briefly, the specimen was placed on a 35-mm culture dish, and 2.0 m*l* of the culture medium containing bacteria was added. The concentration of bacteria was 3 × $10^8$ cells/m*l*. The dish thus prepared was kept in an incubator at 37°C for 48 hr, and the observations of the specimens with a confocal scanning microscope were then performed.

*Cultivation experiments for ATP assay*: As was done in the cultivation experiments, the specimen was cultured in a 35-mm dish for 24 hr with the medium containing bacteria at a concentration 3 × $10^8$ cells/m*l*. Subsequently, we took out the specimen from the dish and rinse away the medium with PBS(–). Then the specimen was transferred to another dish, and 2.0 m*l* of the culture medium supplemented with or without antibiotics was added. The antimicrobial agents were used to investigate the antibiotic resistance of the bacteria enveloped in the biofilm. The specimens were further incubated for another 24 hr in the incubator. The antibiotics utilized were either cefazolin sodium salt (100 $\mu$g/m*l*; Fujisawa, Osaka, Japan) or gentamicin sulfate (50 $\mu$g/m*l*; MP Biomedicals, Aurora, OH, U.S.A.). In the preparatory experiment, susceptibility of the bacteria to the antibiotics had been examined with the disk diffusion method [5]. We had observed a circular zone of inhibition surrounding a paper disk impregnated with gentamicin for all cases of *S. aureus, S. epidermidis*, and *P. aeruginosa*. On the other hand, a zone of inhibition surrounding cefazolin was resulted for *S. aureus* and *S. epidermidis* but not for *P. aeruginosa*. Hence the bacteria used in this experiment were susceptible to the utilized antibiotics, except the case of *P. aeruginosa* to cefazolin.

*CLSM observations*: The formation of biofilm was confirmed by the observation with a CLSM [1, 2, 4, 26, 30].

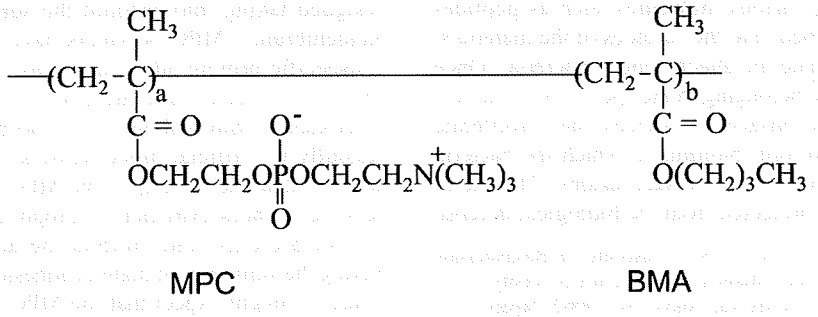


Fig. 1. Chemical formula of poly [MPC-co-n-butyl methacrylate (BMA)] (PMB) used in this study.

After cultivation with bacteria, the specimen was rinsed with PBS(–) and immersed into a 2.5% glutaraldehyde solution for 2 hr for fixation. The specimens were rinsed with PBS(–) again and immersed into an ethidium bromide solution (2 $\mu$g/m*l*; Molecular Probes, Carlsbad, CA, U.S.A.) for 5 min for the staining of bacterial nucleic acid in biofilms [26]; they were then immersed into a fluorescein isothiocyanate (FITC)-conjugated concanavalin A solution (50 $\mu$g/m*l*; Sigma-Aldrich, St. Louis, MO, U.S.A.) for 3 min for the staining of polysaccharides in biofilms [1, 30]. A CLSM (LSM 5 PASCAL; Carl Zeiss MicroImaging GmbH, Jena, Germany) was used for fluorescent observation. The observation was carried out for 10 specimens.

*Measurement of the number of bacteria by ATP assay*: An ATP-dependent luminescence reaction between luciferin and luciferase was utilized to count the number of bacteria [20, 21]. After incubation, the specimen was rinsed with PBS(–). Subsequently, ATP in the bacterial cytoplasm was extracted by sonication for 10 min from the specimen immersed in 0.5 m*l* of 0.5% trichloroacetic acid solution. The amount of ATP was measured using an ATP assay kit (ENLITEN ATP Assay System Bioluminescence Detection Kit; Promega, Madison, WI, U.S.A.) and a luminometer (Auto Lumat; EG&G Berthold, Bad Wildbad, Germany). The relations between the number of bacteria measured by a hemocytometer for bacterial counting (A161; SLGC, Tokyo, Japan) and the relative light unit (RLU) measured by the ATP assay system were established for the respective bacteria. Utilizing these standard relations, the RLU values measured in the experiments were converted to the numbers of bacteria. The measurements were carried out for 10 specimens.

*Statistical analysis*: The obtained data were analyzed by two-way ANOVA to determine the effectiveness of PMB coating and antibiotics in decreasing the number of bacteria. Subsequently, statistical differences among cases in the noncoated and PMB-coated surfaces were examined by Scheffe's multiple comparison test.

## RESULTS

*CLSM observation*: Figure 2 shows the example of a typical observation by CLSM. In every case of exposure to *S. aureus*, *S. epidermidis*, and *P. aeruginosa*, many bacteria and polysaccharides were revealed to exist on the noncoated surfaces of the specimens, as shown in Figs. 2(a), 2(c), and 2(e). On the other hand, there was little or no trace of bacteria or polysaccharides on MPC-coated surfaces, as shown in Figs. 2(b), 2(d), and 2(f). Accordingly, we concluded that biofilm was formed on the noncoated surfaces whereas no biofilm was formed on MPC-coated surfaces.

*Number of bacteria measured by ATP assay*: The ATP assay was performed to measure the number of bacteria and the data are presented in Table 1. Furthermore, statistical analysis was carried out and significant differences between the experimental groups were examined. The analyzed results are illustrated in Fig. 3. In the cases of *S. aureus* and *S. epidermidis*, application of either kind of antibiotics decreased the number of bacteria on the noncoated surfaces ($p<0.01$). On the PMB-coated surfaces, their numbers were smaller than those on the noncoated surfaces ($p<0.01$). The application of antibiotics further decreased the number ($p<0.01$). In the cases of *P. aeruginosa*, application of gentamicin decreased the number ($p<0.01$) whereas cefazolin increased the number of bacteria ($p<0.01$) on the noncoated surfaces. On the PMB-coated surfaces, their numbers were smaller than those on the noncoated surfaces ($p<0.01$). The application of gentamicin decreased the number ($p<0.01$) whereas cefazolin increased the number ($p<0.01$).

## DISCUSSION

Device-associated infections are caused by the bacteria adhered to internal prosthetic devices and are thought to occur through many critical steps [3, 7, 10, 18, 22]. These steps are as follows: adsorbance of various molecules, including peptides and proteins, onto the surfaces of the devices; the mediation of bacterial attachment via these molecules; and the formation of biofilms. If biofilm formation is completed, the bacteria in the biofilm are protected from the biological defense mechanism, and furthermore, from the administered antibacterial agents. Hence, the formation of biofilms on the surface of devices establishes a refractory infection, i.e., device-associated infections [6, 8, 19, 24, 27, 28].

The MPC polymer has the phospholipid polar group and the methacryloyl group in its molecular structure. This confers MPC excellent polymerization ability. The MPC polymers have desirable properties for the inhibition of protein adsorption and cell adhesion. Recently, the MPC polymer was utilized for the coating of medical devices such as artificial blood vessels, implantable artificial hearts, and artificial lungs and successful preventions of thrombus formation were reported [13–17, 25]. Since the attachment of bacteria to the material's surface is also mediated by adsorbed proteins, MPC might be most favorably utilized to inhibit the formation of biofilms. In this investigation, we utilized the PMB as an MPC polymer for the coating materials of metallic specimens to explore the possible uses for the prevention of device-associated infections.

*S. aureus, S. epidermidis*, and *P. aeruginosa* were chosen for this experiment since these bacteria are the most common species causing device-associated infections in the field of orthopedics, and they are also implicated in the pathogenesis of osteomyelitis [10]. Their cultivation was performed following the biofilm formation assay established in previous reports [1, 9, 27, 30]. Then the specimens were stained with ethidium bromide for bacterial nucleic acid and (FITC)-conjugated concanavalin A for polysaccharides and examined by a CLSM, which was also adopted in the biofilm formation assay [1, 26, 30].

In the experiments, the observations by a CLSM clearly demonstrated the presence of bacteria and the existence of polysaccharides on the noncoated surfaces of specimens, as

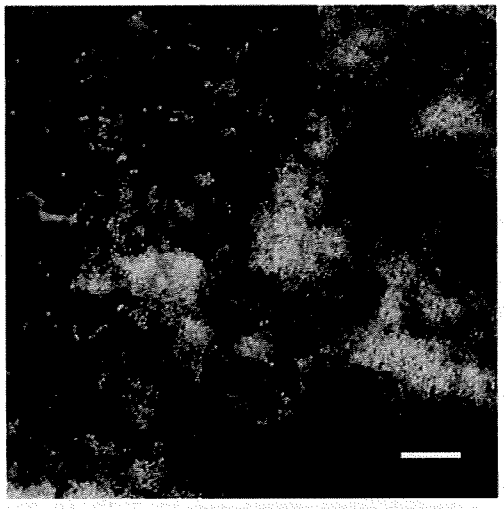

(a) *S. aureus* on noncoated surface

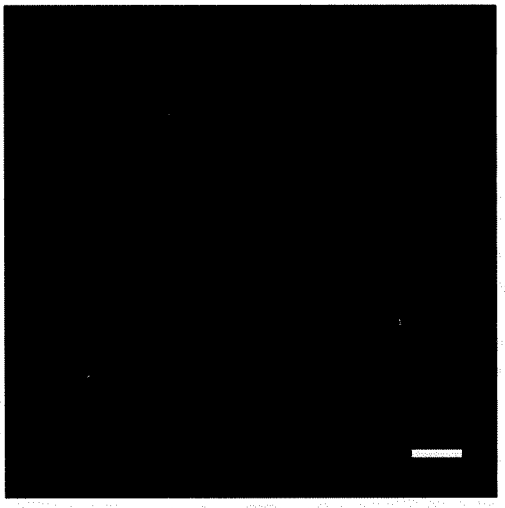

(b) *S. aureus* on PBM-coated surface

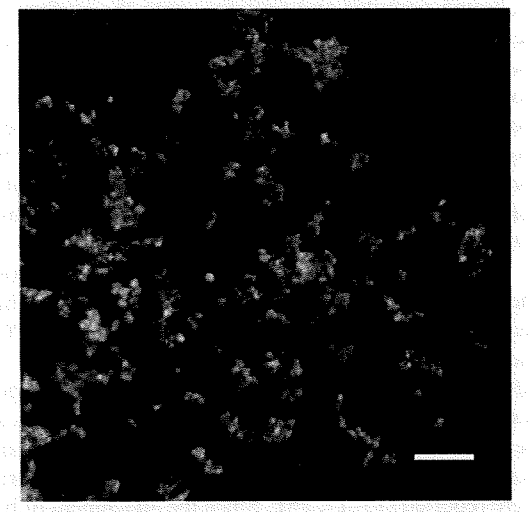

(c) *S. epidermidis* on noncoated surface

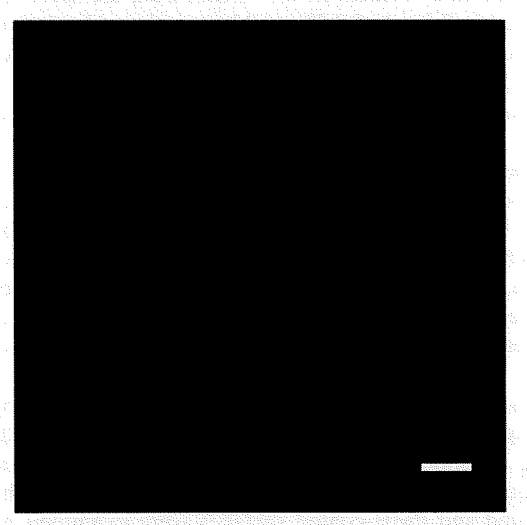

(d) *S. epidermidis* on PMB-coated surface

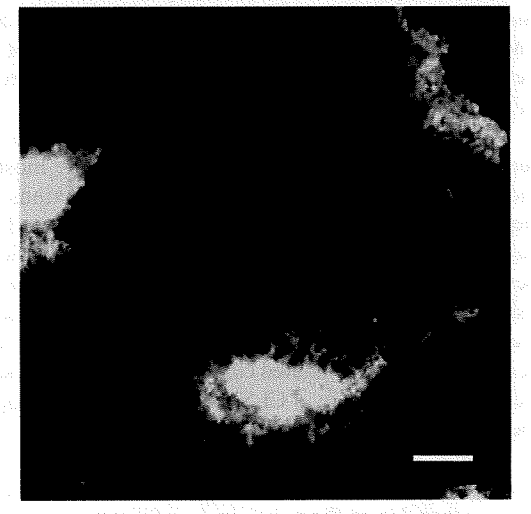

(e) *P. aeruginosa* on noncoated surface

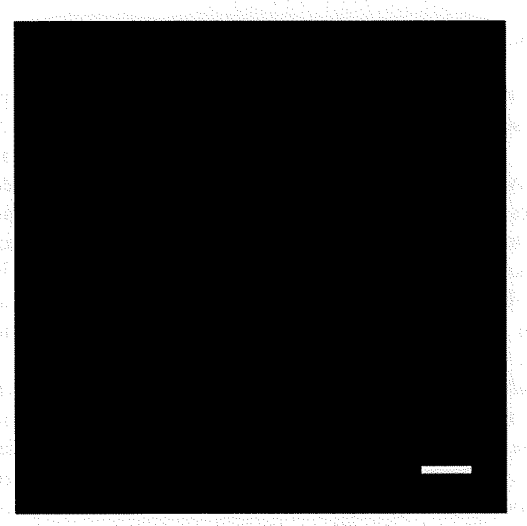

(f) *P. aeruginosa* on PMB-coated surface

Table 1. Number of bacteria ($10^5$ cells/specimen) on noncoated and PMB-coated surfaces on specimens after 24 hr incubation in which antibiotics were absent or either cefazolin or gentamicin were added, following 24 hr incubation without antibiotics. The values are represented as mean ± SD

| coating antibiotics | none | none cefazolin | gentamicin | none | PMB coating cefazolin | gentamicin |
|---|---|---|---|---|---|---|
| S. aureus | 2702 ± 303 | 1722 ± 200 | 1621 ± 91 | 163.3 ± 9.6 | 1.469 ± 0.305 | 1.263 ± 0.134 |
| S. epidermidis | 41.99 ± 6.27 | 1.677 ± 0.186 | 1.789 ± 0.249 | 0.8291 ± 0.1099 | 0.4283 ± 0.0486 | 0.3172 ± 0.0357 |
| P. aeruginoza | 2008 ± 263 | 6080 ± 385 | 1278 ± 295 | 29.74 ± 2.12 | 48.92 ± 2.37 | 9.209 ± 0.345 |

shown in Figs. 2(a), 2(c), and 2(e), which provided a morphological evidence of the formation of biofilms.

The number of bacteria was measured by the ATP assay, and it was demonstrated that the number of bacteria on the noncoated surface of the specimens decreased with statistical significance following the application of cefazolin or gentamicin in the cases of *S. aureus*, as shown in Fig. 3(a). However, the application of antibiotics did not even halve the number of bacteria. The number of *P. aeruginosa* was not halved by the antibiotics in a similar manner as shown in Fig. 3(c). Contrastively, the number of bacterial was increased when they were cultivated in the cefazolin added medium. This might be attributed to that the specimens were incubated for 24 hr in medium without antibiotics and then they were incubated for another 24 hr in new medium containing cefazolin, to which *P. aeruginosa* was not susceptible. In either case of bacteria, anyhow, the fact that antibiotics could not halve the bacteria provided a functional evidence of the formation of biofilms, in which the bacteria were enveloped and protected from the antibiotics. On the other hand, the number of *S. epidermidis* bacteria on the noncoated surface was decreased to less than 1/10 times of the original number by the application of the antibiotics, as shown in Fig. 3(b). The biofilms formed by *S. epidermidis* were seemingly less effective in protecting the bacteria.

In contrast, on the PMB-coated surfaces, the bacteria and polysaccharides were not detected by confocal laser microscopy, as shown in Figs. 2(b), 2(d), and 2(f); this provided a morphological evidence of the absence of biofilms.

The ATP assay demonstrated that the number of bacteria on the PMB-coated surfaces of the specimens decreased with statistical significance compared to those on noncoated surfaces. Although the number of bacteria decreased approximately only 1/20 times the original number in the cases of *S. aureus*, the application of antibiotics further decreased the number of bacteria to approximately 1/2000 times, as shown in Fig. 3(a). This phenomenon proved that the bacteria are not protected from antibiotics and implies that *S. aureus* on the PMB-coated surface, which could not be removed by rinsing, did not form a biofilm. Similarly, the number of *S. epidermidis* was decreased to approximately 1/50 times the original number on the PMB-coated surface, and the application of antibiotics further decreased the number to approximately 1/1200 times, as shown in Fig. 3(b). The number of *P. aeruginosa* was decreased to approximately 1/70 times on a PMB-coated surface, and the application of gentamicin further decreased the number to approximately 1/220 times, but cefazolin was not effective in reducing the number of bacteria, as shown in Fig. 3(c). The difference in the response toward cefazolin and gentamicin is explained by the fact that cefazolin is a beta-lactam antibiotic, which is active against gram-positive bacteria such as *Staphylococcus* sp. but not against *P. aeruginosa*, and gentamicin is an amino-glycoside antibiotic that is active against gram-negative bacteria, including *P. aeruginosa* as well as gram-negative bacteria.

Hence, the observed decreases in the number of bacteria by the application of antibiotics provided a functional evidence that PMB coating prevented the formation of biofilms.

Thus, we concluded that the PMB coating effectively prevented the formation of bacterial biofilms on the surface of metallic specimens. Although our results were limited to *in vitro* experiments and further investigations are necessary, the decrease in the number of bacteria in the order of 1/100 to 1/1,000 is encouraging. We expect that the PMB coating combined with validated uses of antibiotics might provide an effective approach to the simultaneous achievement of a biocompatible surface of devices and the prevention of the device-associated infections.

Further investigations are necessary to achieve successful clinical applications. One of the issues to be examined is, durability of the coating. Yoneyama [32] implanted the MPC polymer coated artificial vessels made of polyester fibers to carotid arteries of rabbit, and observed the antithrombogenicity as long as 4 weeks after implantation. We confirmed the prevention of biofilm forming with the use of PMB coating in 48 hr experiments; however, verification of the durability should be performed. Furthermore, the toxicity of the polymer eluted from the coating layer should be examined.

Fig. 2. CLSM observations of the specimens with noncoated and PMB-coated surfaces after 48 hr incubation. (a). *S. aureus* on noncoated surface, (b) *S. aureus* on PMB-coated surface, (c) *S. epidermidis* on noncoated surface, (d) *S. epidermidis* on PMB-coated surface, (e) *P. aeruginosa* on noncoated surface, (f) *P. aeruginosa* on PMB-coated surface. The nucleic acid in bacteria was stained with ethidium bromide (red) and polysaccharide by FITC conjugated concanavalin A (green). Bar is 10 $\mu$m. Many bacteria and polysaccharides were detected on the noncoated surfaces, whereas they were very few on PMB-coated surfaces.

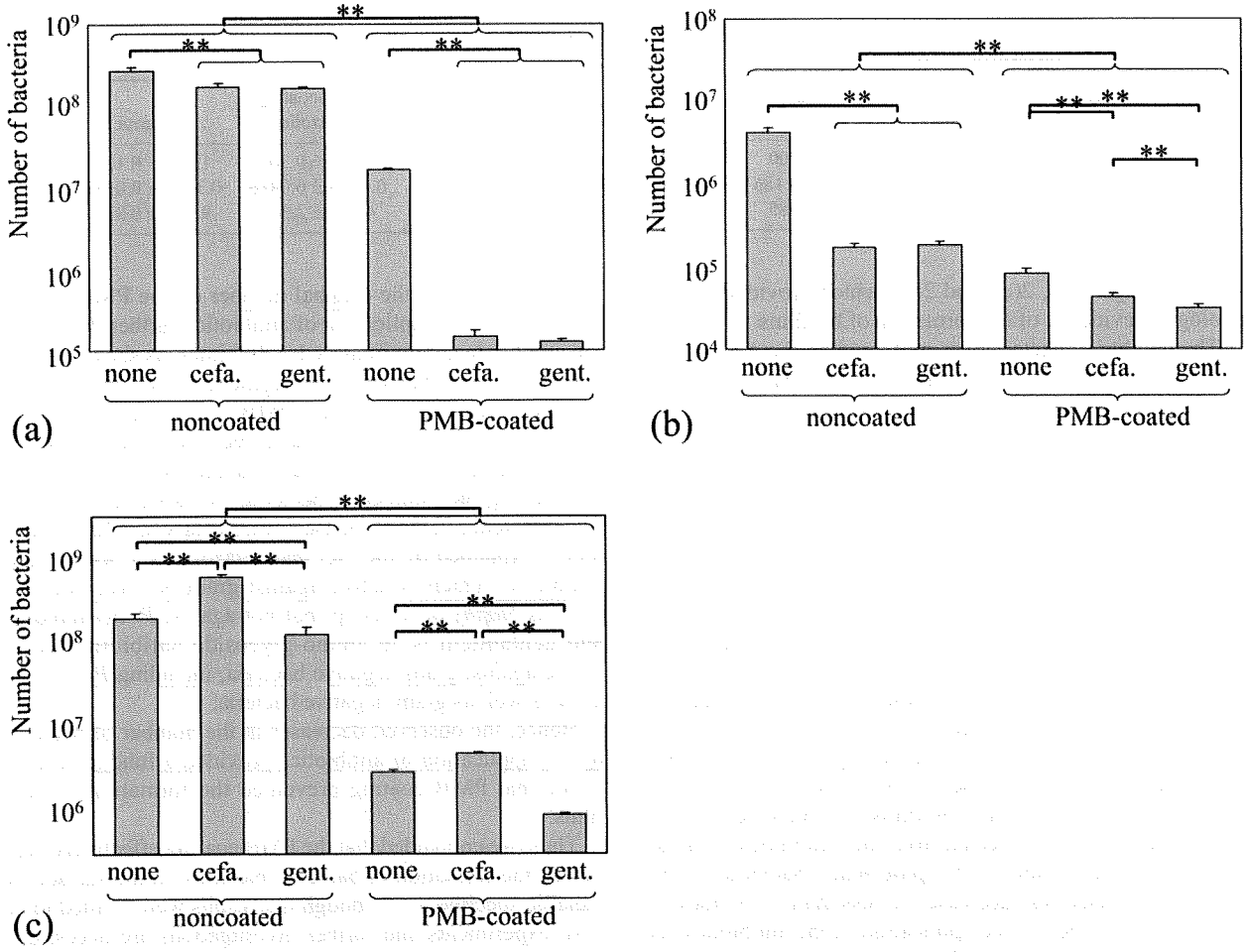


Fig. 3. Number of bacteria on noncoated and PMB-coated surfaces of specimens after 24 hr incubation in which antibiotics were absent or either cefazolin or gentamicin were added, following 24 hr incubation without antibiotics. (a) *S. aureus*, (b) *S. epidermidis*, (c) *P. aeruginosa*.

(a) Number of *S. aureus* on the surfaces on specimens. ** Significant difference ($p<0.01$) was observed; between noncoated and PMB-coated surfaces; between cases in which antibiotics were either absent or present on the noncoated and PMB-coated surfaces.

(b) Number of *S. epidermidis* on the surfaces on specimens. ** Significant difference ($p<0.01$) was observed; between noncoated and PMB-coated surfaces; between cases in which antibiotics were absent and cefazolin and gentamicin were added on the PMB-coated surfaces.

(c) Number of *P. aeruginosa* on the surfaces on specimens. ** Significant difference ($p<0.01$) was observed; between noncoated and PMB-coated surfaces; between cases in which antibiotics were absent, cefazolin and gentamicin were added on the noncoated and PMB-coated surfaces.

ACKNOWLEDGEMENT. This study was partially supported by Grants-in-Aid for Scientific Research on Priority Area (No.15086206) from the Ministry of Education, Culture, Sports, Science and Technology of Japan.

REFERENCES

1. Akiyama, H., Huh, W. K. and Fujii, K. 2002. Confocal laser microscopic observation of glycocalyx production by *Staphylococcus* aureus *in vitro*. *J. Dermatol. Sci.* **29**: 54–61.
2. Caldwell, D. E., Korber, D. R. and Lawrence, J. R. 1992. Confocal laser microscopy and digital image analysis. *Adv. Microb. Ecol.* **12**: 1–67.
3. Chang, C. C. and Merritt, K. 1994. Infection at the site of implanted materials with and without preadhered bacteria. *J. Orthop. Res.* **12**: 526–531.
4. Costerton, J. W., Lewandowski, Z., Caldwell, D. E., Korber, D. R. and Lappin-Scott, H. M. 1995. Microbial biofilms. *Annu. Rev. Microbiol.* **49**: 711–745.
5. Felten, A., Grandry, B., Lagrange, P. H. and Casin, I. 2002. Evaluation of three techniques for detection of low-level methicillin-resistant *Staphylococcus aureus* (MRSA): a disk diffusion method with cefoxitin and moxalactam, the Vitek 2 System, and the MRSA-Screen Latex Agglutination Test. *J. Clin. Micorbiol.* **40**: 2766–2771.
6. Gristina, A. G. 1987. Biomaterial centered infection. Microbial adhesion versus tissue integration. *Science* **27**: 1588–1595.
7. Harris, L. G., Foster, S. J. and Richards, R. G. 2002. An introduction to *Staphylococcus aureus*, and techniques for identify-

ing and quantifying *S. aureus* adhesions in relation to adhesion to biomaterials: review. *Eur. Cell Mater.* **4**: 39–60.
8. Harris, L. G., Tosatti, S. and Wieland, M. 2004. *Staphylococcus aureus* adhesion to titanium oxide surfaces coated with non-functionized poly(L-lysine)-grafted- poly(ethylene glycol) copolymers. *Biomaterials* **25**: 4135–4148.
9. Hirota, K., Murakami, K. and Nemoto, K. 2005. Coating of a surface with 2-methacryloyloxyethyl phosphorylcholine (MPC) co-polymer significantly reduces retention of human pathogenic microorganisms. *FEMS Microbiol. Lett.* **248**: 37–45.
10. Hudson, M. C., Ramp, W. K. and Frankenburg, K. P. 1999. *Staphylococcus aureus* adhesion to bone matrix and bone-associated biomaterials. *FEMS Microbiol. Lett.* **173**: 279–284.
11. Hussain, M., Hasting, J. G. and White, P. J. 1991. Isolation and composition of the extracellular slime made by coagulase-negative staphylococci in a chemically defined medium. *J. Infect. Dis.* **163**: 534–541.
12. Ishihara, K., Fukumoto, K., Iwasaki, Y. and Nakabayashi, N. 1999. Modification of polysulfone with phospholipid polymer for improvement of the blood compatibility. Part 1. Surface characterization. *Biomaterials* **20**: 1545–1551.
13. Ishihara, K., Oshida, H. and Endo, Y. 1992. Hemocompatibility of human whole blood on polymers with a phospholipid polar group and its mechanism. *J. Biomed. Mater. Res.* **26**: 1543–1552.
14. Ishihara, K., Ueda, T. and Nakabayashi, N. 1990. Preparation of phospholipid polymers and their properties as polymer hydrogel membranes. *Polym. J.* **22**: 355–360.
15. Ishihara, K., Ziats, N. P. and Tierney, B. P. 1991. Protein adsorption from human plasma is reduced on phospholipid polymers. *J. Biomed. Mater. Res.* **25**: 1397–1407.
16. Iwasaki, Y. and Ishihara, K. 2005. Phosphorylcholine-containing polymers for biomedical applications. *Anal. Bioanal. Chem.* **381**: 534–546.
17. Iwasaki, Y., Nakabayashi, N. and Ishihara, K. 2003. *In vitro* and *ex vivo* blood compatibility study of 2-methacryloyloxyethyl phosphorylcholine (MPC) copolymer-coated hemodialysis hollow fibers. *J. Artif. Organs* **6**: 260–266.
18. Jeanine, A., Jaques, O. G. and Anne, M. 1999. Tracking adhesion factors in *Staphylococcus caprae* strains responsible for human bone infections following implantation of orthopaedic material. *Microbiology* **145**: 2033–2042.
19. Jennings, D. A., Morykwas, M. J., Burns, W. W., Crook M. E., Hudson, W. P. and Argenta, L. C. 1991. *In vitro* adhesion of endogenous skin microorganism to breast prostheses. *Ann. Plast. Surg.* **27**: 216–220.
20. Lundin, A. and Thore, A. 1975. Analytical information obtainable by evaluation of the time course of firefly bioluminescence in the assay of ATP. *Anal. Biochem.* **66**: 47–63.
21. McElroy, W. D. and DeLuca, M. A. 1983. Firefly and bacterial luminescence. Basic science and applications. *J. Appl. Biochem.* **5**: 197–209.
22. Merritt, K. and Chang, C. C. 1991. Factors influencing bacterial adherence to biomaterials. *J. Biomater. Appl.* **5**: 185–203.
23. Merritt, K. and Dowd, J. D. 1987. Role of internal fixation in infection of open fracture: Studies with *Staphylococcus aureus* and *Proteus mirabilis*. *J. Orthop. Res.* **5**: 23–28.
24. Montanaro, L., Arciola, C. R. and Baldassarri, L. 1999. Presence and expression of collagen adhesion gene (can) and slime production in *Staphylpcoccus aureus* strains from orthopaedic prosthesis infection. *Biomaterials* **20**: 1945–1949.
25. Ogawa, R., Watanabe, J. and Ishihara, K. 2003. Domain-controlled polymer alloy composed of segmented polyurethane and phospholipid polymer for biomedical applications. *Sci. Technol. Adv. Mater.* **4**: 523–530.
26. Qian, Z., Stoodley, P. and Pitt, W. G. 1996. Effect of low-intensity ultrasound upon biofilm structure from confocal scanning laser microscopy observation. *Biomaterials* **17**: 1975–1980.
27. Ramage, G., Tunney, M. M. and Patrick, S. 2003. Formation of propinibacterium acnes biofilms on orthopaedic biomaterials and their susceptibility to antimicrobials. *Biomaterials* **24**: 3221–3227.
28. Sheehan, E., McKenna, J. and Mulhall, K. J. 2004. Adhesion of *Staphylococcus* to orthopaedic materials, an *in vivo* study. *J. Orthop. Res.* **22**: 39–43.
29. Takahashi, H. 2001. Examination about the bio-film formation prevention effect of the antibacterial new coating catheter material which blended citrate silver and lecithin. *Kansenshoushi* **75**: 678–685 (in Japanese).
30. Takenaka, S., Iwaku, M. and Hoshino, E. 2001. Artificial *Pseudomonas aeruginosa* biofilm and confocal laser scanning microscopic analysis. *J. Infect. Chemother.* **7**: 87–93.
31. Wassall, M. A., Santin, M. and Isalberti, C. 1997. Adhesion of bacterial to stainless steel and silver-coated orthopedic external fixation pins. *J. Biomed. Mater. Res.* **36**: 325–330.
32. Yoneyama, T., Ito, M., Sugihara, K., Ishihara, K. and Nakabayashi, N. 2000. Small diameter vascular prosthesis with a non-thrombogenic phospholipid polymer surface: preliminary study of a new concept for functioning in the absence of pseudo- or neointima formation. *Artif. Organs* **24**: 23–28.

ARTHRITIS & RHEUMATISM
Vol. 60, No. 1, January 2009, pp 166–178
DOI 10.1002/art.24243


# Identification of the Core Element Responsive to Runt-Related Transcription Factor 2 in the Promoter of Human Type X Collagen Gene

Akiro Higashikawa, Taku Saito, Toshiyuki Ikeda, Satoru Kamekura, Naohiro Kawamura, Akinori Kan, Yasushi Oshima, Shinsuke Ohba, Naoshi Ogata, Katsushi Takeshita, Kozo Nakamura, Ung-il Chung, and Hiroshi Kawaguchi

*Objective.* **Type X collagen and runt-related transcription factor 2 (RUNX-2) are known to be important for chondrocyte hypertrophy during skeletal growth and repair and development of osteoarthritis (OA) in mice. Aiming at clinical application, this study was undertaken to investigate transcriptional regulation of human type X collagen by RUNX-2 in human cells.**

*Methods.* **Localization of type X collagen and RUNX-2 was determined by immunohistochemistry, and their functional interaction was examined in cultured mouse chondrogenic ATDC-5 cells. Promoter activity of the human type X collagen gene (COL10A1) was examined in human HeLa, HuH7, and OUMS27 cells transfected with a luciferase gene containing a 4.5-kb promoter and fragments. Binding to RUNX-2 was examined by electrophoretic mobility shift assay and chromatin immunoprecipitation.**

*Results.* **RUNX-2 and type X collagen were colocalized in mouse limb cartilage and bone fracture callus. Gain and loss of function of RUNX-2 revealed that RUNX-2 is essential for type X collagen expression and terminal differentiation of chondrocytes. Human COL10A1 promoter activity was enhanced by RUNX-2 alone and more potently by RUNX-2 in combination with the coactivator core-binding factor $\beta$ in all 3 human cell lines examined. Deletion, mutagenesis, and tandem repeat analyses identified the core responsive element as the region between −89 and −60 bp (termed the hypertrophy box [HY box]), which showed specific binding to RUNX-2. Other putative RUNX-2 binding motifs in the human COL10A1 promoter did not respond to RUNX-2 in human cells.**

*Conclusion.* **Our findings indicate that the HY box is the core element responsive to RUNX-2 in human COL10A1 promoter. Studies on molecular networks related to RUNX-2 and the HY box will lead to treatments of skeletal growth retardation, bone fracture, and OA.**

Hypertrophic differentiation of chondrocytes during endochondral ossification is an essential step in skeletal growth and repair (1,2). We and others have reported that chondrocyte hypertrophy also contributes to cartilage degradation during the development of osteoarthritis (OA) (3–5). Type X collagen is a short, network-forming collagen specifically expressed by hypertrophic chondrocytes (6). The physiologic importance of type X collagen has been shown by the impairment of endochondral ossification and skeletal growth that results from loss of function of the type X collagen gene in mice (7–9). Similarly, mutations in the carboxy-terminal domain of the human type X collagen gene (COL10A1) cause a severe skeletal disorder called Schmid-type metaphyseal chondrodysplasia, with growth retardation, waddling gait, and OA (10–12). Hence, elucidation of the mechanisms regulating the type X collagen gene will contribute to understanding the molecular backgrounds of skeletal growth and repair and OA not only in mice, but also in humans.

Supported by a Grant-in-Aid for Scientific Research from the Japanese Ministry of Education, Culture, Sports, Science, and Technology (18659435).

Akiro Higashikawa, MD, Taku Saito, MD, PhD, Toshiyuki Ikeda, MD, Satoru Kamekura, MD, PhD, Naohiro Kawamura, MD, PhD, Akinori Kan, MD, Yasushi Oshima, MD, PhD, Shinsuke Ohba, PhD, Naoshi Ogata, MD, PhD, Katsushi Takeshita, MD, PhD, Kozo Nakamura, MD, PhD, Ung-il Chung, MD, PhD, Hiroshi Kawaguchi, MD, PhD: University of Tokyo, Tokyo, Japan.

Address correspondence and reprint requests to Hiroshi Kawaguchi, MD, PhD, Sensory and Motor System Medicine, Faculty of Medicine, University of Tokyo, Hongo 7-3-1, Bunkyo, Tokyo 113-8655, Japan. E-mail: kawaguchi-ort@h.u-tokyo.ac.jp.

Submitted for publication August 9, 2008; accepted in revised form October 13, 2008.

The specificity of type X collagen expression in hypertrophic chondrocytes underlies tight control by transcriptional regulation of gene expression. Runt-related transcription factor 2 (RUNX-2) was originally isolated on the basis of its ability to transactivate the osteoblast-specific osteocalcin gene and is well known as a key molecule for bone formation (13,14). However, recent in vivo studies in mice have revealed that RUNX-2 is the pivotal transcription factor for type X collagen expression and chondrocyte hypertrophy during endochondral ossification (15–20). RUNX-2 is known to function by forming a heterodimer with a cotranscription factor called core-binding factor $\beta$ (CBF$\beta$) (21).

In a previous study (22,23), we created an experimental OA model by induction of joint instability in mouse knee joints (5). RUNX-2 expression was induced in articular cartilage chondrocytes, followed by type X collagen expression and chondrocyte hypertrophy. Type X collagen expression and cartilage degradation were greatly suppressed in the joints of heterozygous *Runx2*-knockout ($Runx2^{+/-}$) mice as compared with their wild-type littermates. These findings indicate that the RUNX-2–type X collagen signal is likely to play a crucial role in pathologic skeletal disorders, such as OA, as well as in physiologic skeletal growth and repair. Although RUNX-2 has been reported to activate the promoter of the mouse Col10a1 gene directly via its putative RUNX-2 binding motifs (20), the mechanism of transcriptional regulation of the human COL10A1 gene by RUNX-2 remains unknown. Hence, aiming at clinical application of this signal to treatments of skeletal growth retardation, bone fracture, and OA, in this study we investigated the mechanism underlying the transcriptional regulation of human COL10A1 by RUNX-2 in human cells.

## MATERIALS AND METHODS

**Animals.** All experiments were performed according to a protocol approved by the Animal Care and Use Committee of the University of Tokyo. Wild-type and heterozygous *Runx2*-deficient mice with the *lacZ* gene inserted at the site of the *Runx2* gene deletion ($Runx2^{+/lacZ}$) were maintained on a C57BL/6 background and were fed a standard rodent diet (CE-2; Clea, Tokyo, Japan).

**Bone fracture experiment.** A transverse osteotomy was created using a bone saw at the midshaft in the left femur of 8-week-old male $Runx2^{+/lacZ}$ mice, and was internally stabilized with an intramedullary nail using the inner pin of a 22-gauge spinal needle, as previously described (24–26). For histologic analyses, animals were killed by $CO_2$ asphyxiation 9 days after surgery, and femurs were excised.

**Histologic analysis.** Excised tibial limbs and femurs were fixed in 4% formaldehyde buffered with phosphate buffered saline (pH 7.4) for 1 hour at 4°C and rinsed 3 times with washing buffer (0.1*M* sodium phosphate, 0.02% Nonidet P40, 0.01% deoxycholic acid, and 2 m*M* $MgCl_2$ [pH 7.4]). To detect $\beta$-galactosidase activity, tibial limbs and femurs were subsequently stained with X-Gal staining buffer (1 mg/ml X-Gal, 5 m*M* potassium ferricyanide, and 5 m*M* potassium ferrocyanide buffered with the washing buffer described above) for 36 hours. The femurs were additionally decalcified for 2 weeks with 10% EDTA (pH 7.4) at 4°C. After dehydration with an increasing concentration of ethanol and embedding in paraffin, they were sectioned into 4-$\mu$m slices. For immunohistochemistry, after treatment with 25 $\mu$g/ml hyaluronidase for 1 hour, sections were incubated overnight with rabbit polyclonal antibodies to rat type X collagen or with nonimmune serum (1:500 dilution; LSL, Tokyo, Japan). Localizations were detected with a horseradish peroxidase–conjugated secondary antibody (Promega, Madison, WI).

**Construction of expression vectors.** Full-length human RUNX-2 (accession no. NM_004348) complementary DNA (cDNA) and CBF$\beta$ (accession no. NM_022845) cDNA were amplified by polymerase chain reaction (PCR) and cloned into pCMV-HA (Clontech, Palo Alto, CA). RUNX-2 (accession no. NM_009820) cDNA and cDNA for a dominant-negative mutant of RUNX-2 (dnRUNX-2) were cloned into pMx vectors (27). A vector expressing dnRUNX-2 was generated by the form which contains the runt domain with N-terminal domain of RUNX-2 and lacks the C-terminal region, as previously described (19). Production of retrovirus vectors was performed as previously described (28,29). Plat-E cells ($2 \times 10^6$) were plated in 60-mm dishes and transfected with 2 $\mu$g of pMx vector using FuGene 6 (Roche, Mannheim, Germany). After 24 hours, the medium was replaced with fresh medium, which was collected and used as the retrovirus supernatant 48 hours after transfection. The blasticidin resistance gene was inserted into the pMx vector of RUNX-2 and that of dnRUNX-2 for selection of stable cells.

**Cell cultures.** HeLa cells, HuH7 cells, COS-7 cells (RIKEN Cell Bank, Tsukuba, Japan), and OUMS27 cells (Health Science Research Resources Bank, Tokyo, Japan) were cultured in high-glucose Dulbecco's modified Eagle's medium (DMEM) with 10% fetal bovine serum (FBS). ATDC-5 cells (RIKEN Cell Bank) were grown and maintained in DMEM–Ham's F-12 (1:1) with 5% FBS. To induce hypertrophic differentiation, ATDC-5 cells were cultured in the presence of insulin–transferrin–sodium selenite supplement (Sigma, St. Louis, MO) for 3 weeks, and then with $\alpha$-minimum essential medium/5% FBS with 4 m*M* inorganic phosphate for 2 days, as previously described (30). For generation of the stable cell lines, $3 \times 10^5$ ATDC-5 cells were plated and cultured in 60-mm dishes for 1 day, and the retrovirus supernatant was added to the cells with Polybrene (8 $\mu$g/ml final concentration). After 2 days, the cells were passaged into 100-mm dishes and cultured with medium containing 10 $\mu$g/ml blasticidin until confluency. For alizarin red staining, cultured cells were fixed in 10% buffered formalin and stained for 10 minutes with 2% alizarin red S (pH 4.0) (Sigma). For von Kossa's staining, cells were fixed with 100% ethanol for 15 minutes and stained with 5% silver nitrate solution under ultraviolet light for 5 minutes.

**Reverse transcriptase–PCR (RT-PCR) and real-time RT-PCR analyses.** Total RNA from cells was isolated with an RNeasy Mini kit, according to the recommendations of the manufacturer (Qiagen, Hilden, Germany), and 1 aliquot (1 μg) was reverse-transcribed with a QuantiTect Reverse Transcription kit (Qiagen) to make single-stranded cDNA. For RT-PCR, cDNA was amplified for 30 cycles in a PCR thermal cycler using Takara Ex *Taq* (Takara Bio, Shiga, Japan) and the following primer pairs: for the N-terminal region of RUNX-2, 5′-GCAAGATGAGCGACGTGAG-3′ and 5′-GTCCGCGATGATCTCCAC-3′; for the C-terminal region of RUNX-2, 5′-CCCAGCCACCTTTACCTACA-3′ and 5′-TATGGAGTGCTGCTGGTCTG-3′; and for β-actin, 5′-AGATGTGGATCAGCAAGCAG-3′and5′-GCGCAAGTTAGGTTTTGTCA-3′.

Real-time RT-PCR was performed with an ABI Prism 7000 Sequence Detection System (Applied Biosystems, Foster City, CA) using QuantiTect SYBR Green PCR Master Mix, according to the recommendations of the manufacturer (Qiagen). All reactions were run in triplicate. After data collection, the messenger RNA (mRNA) copy number of a specific gene in total RNA was calculated using a standard curve generated with serially diluted plasmids containing PCR amplicon sequences and normalized to rodent total RNA (Applied Biosystems) with mouse β-actin as an internal control. Standard plasmids were synthesized with a TOPO TA cloning kit, according to the recommendations of the manufacturer (Invitrogen, Carlsbad, CA). PCR amplification was performed using the following primer pairs: for type X collagen, 5′-CATAAAGGGCCCACTTGCTA-3′ and 5′-TGGCTGATATTCCTGGTGGT-3′; and for β-actin, 5′-AGATGTGGATCAGCAAGCAG-3′ and 5′-GCGCAAGTTAGGTTTTGTCA-3′.

**Sequence search of COL10A1 promoters.** A sequence search for the RUNX-2 binding motif was performed using Vector NTI (Invitrogen). To search sequences that were conserved between the human and mouse COL10A1 proximal promoters, we performed a BLASTN search (31) against the mouse genomic plus transcript database using a 4.5-kb fragment of the human COL10A1 5′-end flanking region.

**Luciferase assay.** The human COL10A1 promoter region from −4,459 bp to +39 bp relative to the transcription start site was obtained by PCR using human genomic DNA as a template and was cloned into the pGL3-Basic vector (Promega). Deletion and mutation constructs were created by PCR. Tandem repeat constructs were created by ligating double-stranded oligonucleotides into the pGL3-Basic vector. Transfection of HeLa, HuH7, OUMS27, and ATDC-5 cells was performed in triplicate in 48-well plates using FuGene 6 with plasmid DNA (100 ng of pGL3 reporter vector, 50 ng of effector vector, and 4 ng of pRL-TK vector [Promega]) for internal control per well. Cells were harvested 48 hours after transfection. Luciferase assay was performed with a dual luciferase reporter assay system (Promega) using a GloMax 96 microplate luminometer (Promega). Results were shown as the ratio of firefly activity to *Renilla* activity.

**Electrophoretic mobility shift assay (EMSA).** Nuclear extracts were obtained from COS-7 cells overexpressing empty vector, RUNX-2, or the combination of RUNX-2 and CBFβ 48 hours after transfection using NE-PER, according to the recommendations of the manufacturer (Pierce, Rockford, IL). Each expression vector was transfected using FuGene 6. EMSA was carried out using a DIG Gel Shift kit, according to the recommendations of the manufacturer (Roche). Binding reactions were incubated for 30 minutes at room temperature. For competition analyses, a 100-fold excess of unlabeled competitor probe was included in the binding reaction. For the supershift experiments, 1 μl of anti–RUNX-2 antibody (M-70 X; Santa Cruz Biotechnology, Santa Cruz, CA) was added after 30 minutes of binding reaction, and the reaction was incubated for an additional 30 minutes at room temperature. Samples were loaded onto Novex 6% Tris–borate–EDTA gels (Invitrogen) and electrophoresed at 100V for 60 minutes.

**Chromatin immunoprecipitation (ChIP) assay.** A ChIP assay was performed with a OneDay ChIP kit, according to the recommendations of the manufacturer (Diagenode, Liège, Belgium). HuH7 cells were transfected with empty vector and the combination of RUNX-2 and CBFβ using FuGene 6. In vivo crosslinking was performed 48 hours after transfection. To shear genomic DNA, the lysates were then sonicated on ice 10 times for 30 seconds each. For immunoprecipitation, anti–RUNX-2 antibody (M-70 X) and normal rabbit IgG (negative control; Promega) were used.

## RESULTS

**Localization of RUNX-2 and type X collagen during endochondral ossification.** We initially examined the in vivo expression patterns of RUNX-2 and type X collagen during endochondral ossification in skeletal growth and repair using specimens of limb cartilage from neonatal mice and bone fracture callus from adult mice (Figure 1). Due to the lack of appropriate and sensitive antibodies or riboprobes to examine RUNX-2 localization in wild-type mouse cartilage tissue, we used X-Gal staining in heterozygous *Runx2*-deficient mice with the *lacZ* gene insertion at the *Runx2*-deletion site ($Runx2^{+/lacZ}$) (32). RUNX-2 was widely expressed in cartilage and bone areas, but was expressed most strongly in hypertrophic chondrocytes in both specimens. Strong RUNX-2 expression was well colocalized with the area of positive immunostaining with type X collagen, consistent with the results we previously reported for OA cartilage (22) and confirming the molecular interaction between RUNX-2 and type X collagen during endochondral ossification.

**Functional role of RUNX-2 in type X collagen expression and terminal differentiation of cultured chondrocytes.** To investigate the function of RUNX-2 during endochondral ossification, we examined the effects of gain and loss of function of RUNX-2 on mouse chondrogenic ATDC-5 cells that were cultured in differentiation medium (30). For the gain-of-function analysis, we established stable lines of ATDC-5 cells overexpressing RUNX-2 or the empty vector through retroviral

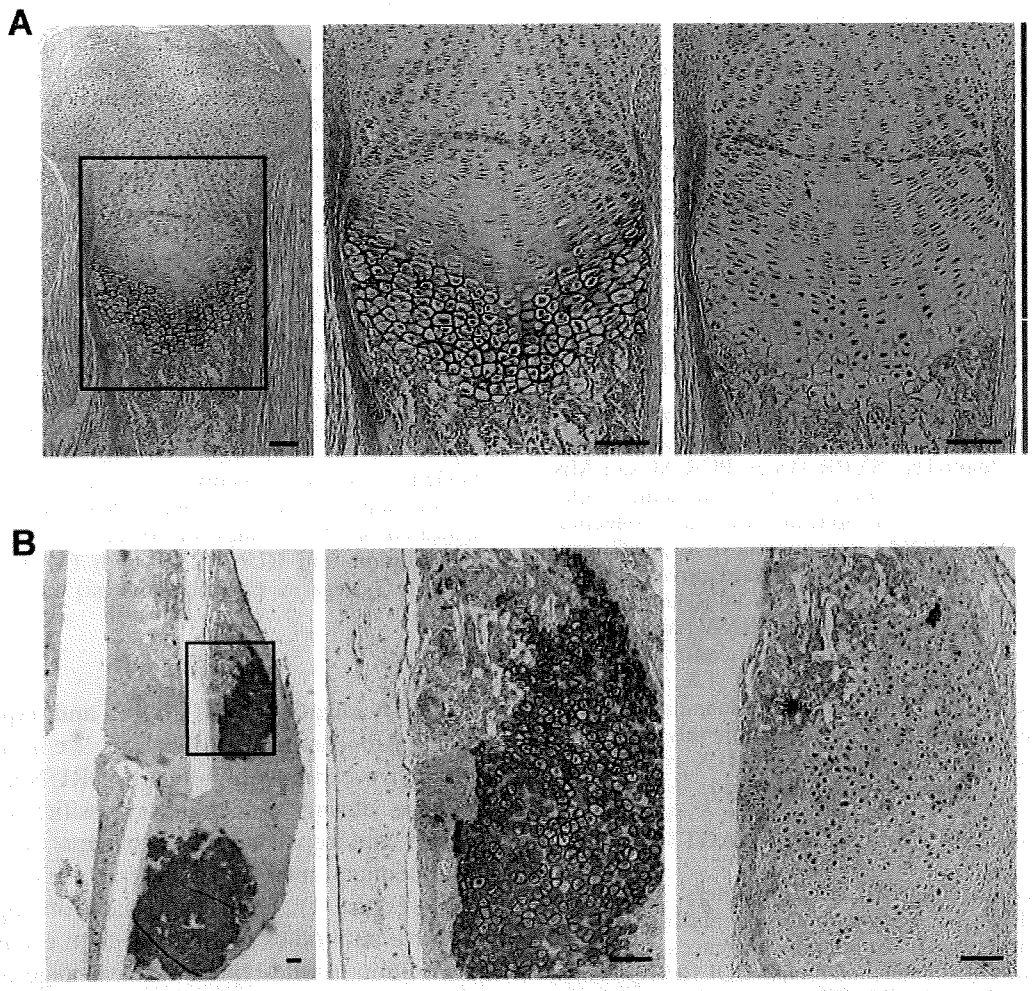


**Figure 1.** Expression of runt-related transcription factor 2 (RUNX-2) and type X collagen in **A,** the proximal tibial limb cartilage of 1-day-old neonatal mice and **B,** the bone fracture callus of 8-week-old adult mice 9 days after osteotomy at the femur midshaft. Specimens from heterozygous *Runx2*-deficient mice with the RUNX-2 promoter and *lacZ* gene knockin at the *Runx2* deletion site ($Runx2^{+/lacZ}$ mice) were stained with X-Gal and antibody to type X collagen (left and middle) or with X-Gal and nonimmune control serum (right). RUNX-2 localization is shown as blue X-Gal staining to detect $\beta$-galactosidase activity. Type X collagen localization is shown as brown immunostaining with an antibody to type X collagen. The middle and right panels show higher-magnification views of the boxed areas in the left panels. The blue, red, and green bars in **A** indicate layers of proliferative zone, hypertrophic zone, and bone area, respectively. Bars = 100 $\mu$m.

transfection and found that the type X collagen mRNA level as well as the terminal differentiation determined by alizarin red and von Kossa's stainings were potently stimulated by RUNX-2 overexpression (Figure 2A).

Next, to determine the effects of loss of function of RUNX-2, we established stable lines of ATDC-5 cells overexpressing a dominant-negative mutant of RUNX-2 that lacks the C-terminal region (19), which were cultured in differentiation medium (Figure 2B). The type X collagen mRNA level and the intensity of the stainings were decreased by the overexpression, indicating that RUNX-2 is a crucial factor for type X collagen expression and terminal differentiation of chondrocytes.

**Transactivation of the human COL10A1 promoter by RUNX-2 and identification of the responsive element.** To examine the mechanism underlying the induction of type X collagen expression by RUNX-2 in humans, we initially compared sequences of the 4.5-kb fragment of the 5′-end flanking region of the human COL10A1 gene with the corresponding mouse genes

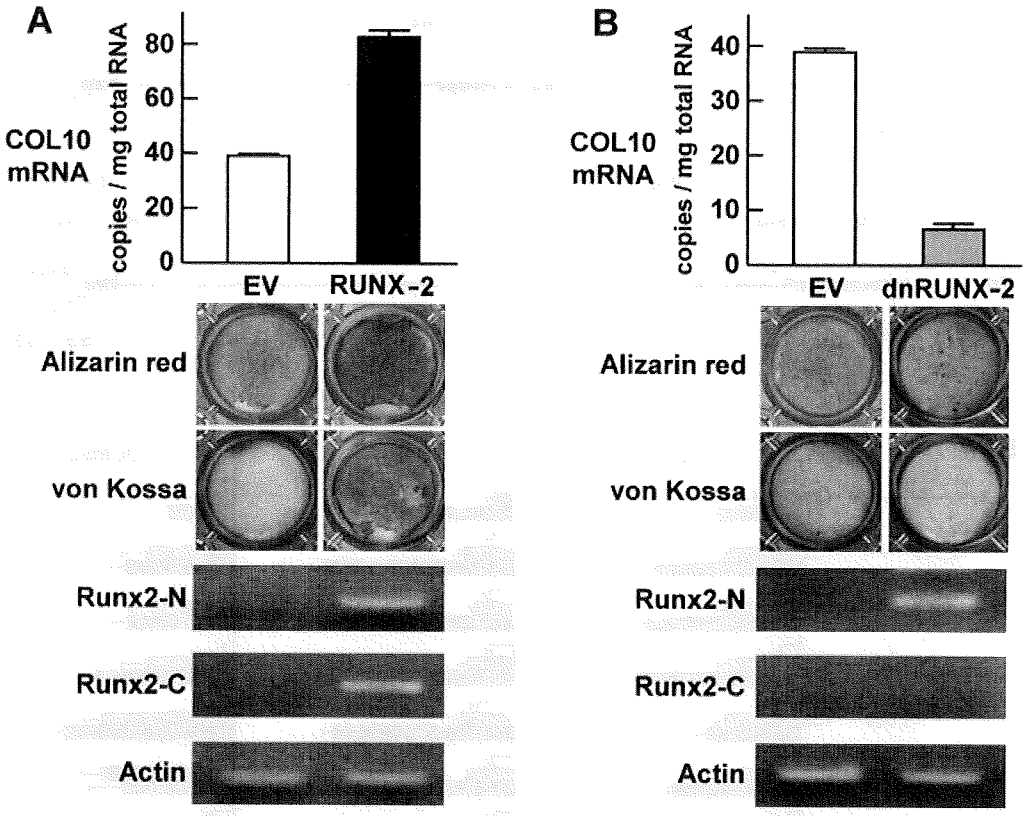


**Figure 2.** Effect of gain and loss of function of runt-related transcription factor 2 (RUNX-2) on type X collagen (COL10) expression and terminal differentiation in cultured mouse chondrogenic ATDC-5 cells. **A,** Type X collagen mRNA level, determined by real-time reverse transcriptase–polymerase chain reaction (RT-PCR), and alizarin red and von Kossa's staining in stable lines of ATDC-5 cells retrovirally transfected with empty vector (EV; control) or with RUNX-2 after culture for 3 weeks with insulin–transferrin–sodium selenite and for 2 days with inorganic phosphate. **B,** Type X collagen mRNA level, determined by RT-PCR, and alizarin red and von Kossa's staining in stable lines of ATDC-5 cells retrovirally transfected with empty vector or with dominant-negative RUNX-2 (dnRUNX-2), which contains the N-terminal region (Runx2-N), but not the C-terminal region (Runx2-C) of RUNX-2, under the same culture conditions as in **A.** Gene expression of RUNX-2 and dnRUNX-2 was confirmed by RT-PCR analysis using 2 primer sets for the N-terminal region and the C-terminal region of RUNX-2. Bars show the mean and SD of 3 wells per group.

(Figure 3A). The sequences were substantially different, except for 2 regions that were ≥70% conserved between the species.

We then analyzed the promoter activity of the human COL10A1 gene using 3 human cell lines, epithelial HeLa cells, hepatic HuH7 cells, and chondrogenic OUMS27 cells, that were transfected with a luciferase reporter gene construct containing the 4.5-kb fragment of the 5′-end flanking region of the COL10A1 gene and the series of deletion fragments (Figure 3B). The transcription activity determined by the luciferase reporter assay was enhanced by cotransfection with RUNX-2 and more potently by cotransfection with both RUNX-2 and the coactivator CBFβ as compared with the control empty vector, confirming activation of the COL10A1 promoter by RUNX-2 and enhancement by the CBFβ cotransfection in all cell lines. Deletion analysis by a series of 5′-deletion constructs identified the responsive region to RUNX-2 as being between −81 bp and −76 bp, containing a putative RUNX-2 binding sequence (TGAGGG), which is similar to that identified in the promoter region of human interleukin-3 (TGTGGG) (33). This was within the highly conserved region in the comparative mapping described above (Figure 3A).

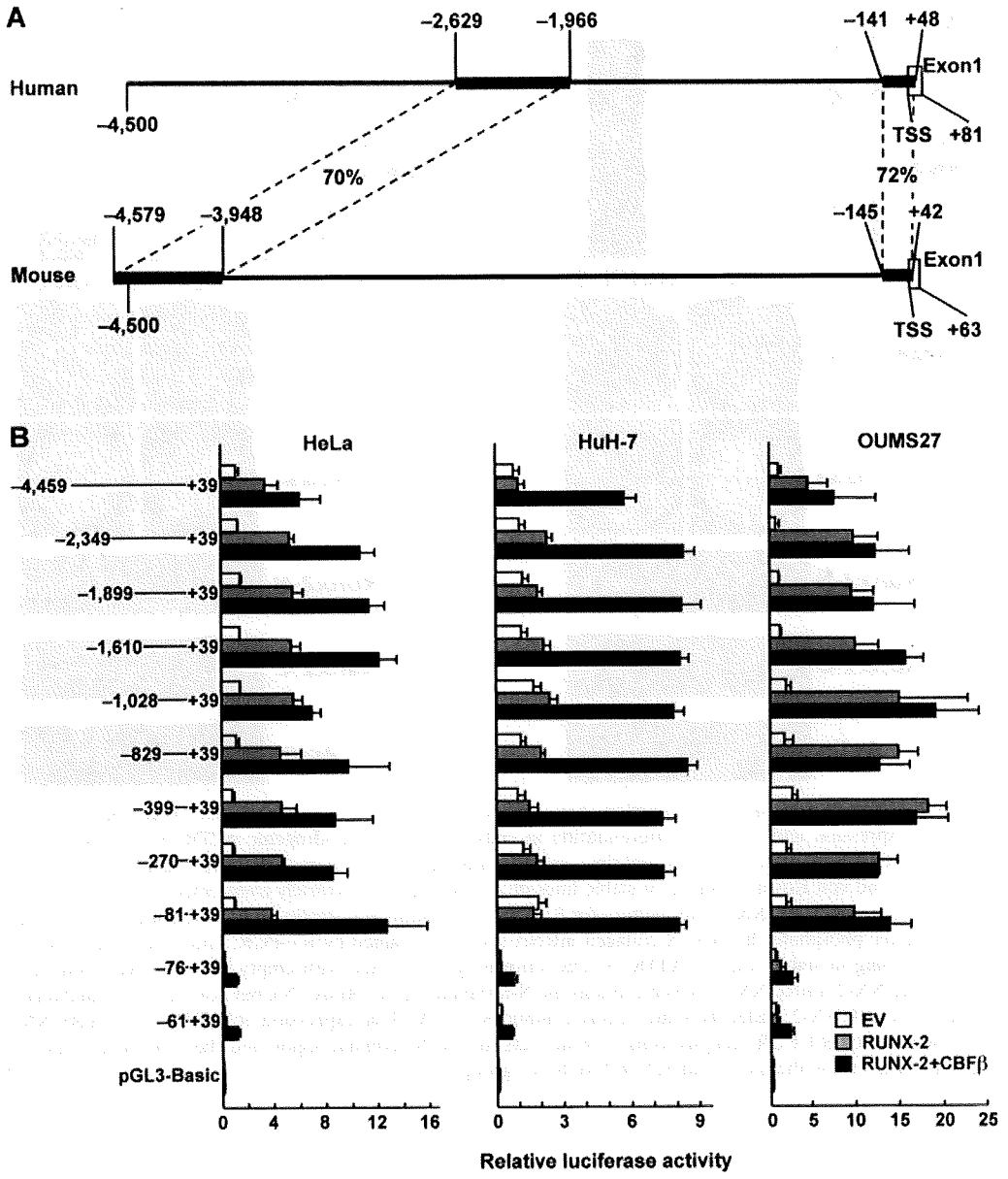


**Figure 3.** **A,** Comparison of sequences of COL10A1 proximal promoter regions in human and mouse genes. The 4.5-kb fragment of the human 5′-end flanking region was compared with the mouse genomic plus transcript database. **B,** Luciferase assays for human COL10A1 promoter activity induced by transfection with RUNX-2 and identification of the responsive region by deletion analysis in human cells. Three human cell lines, epithelial HeLa cells, hepatic HuH7 cells, and chondrogenic OUMS27 cells, transfected with luciferase reporter constructs containing a 5′-end flanking region of the human COL10A1 gene (from −4,459 bp to +39 bp relative to the transcription start site) and the series of deletion fragments were cotransfected with empty vector (control), RUNX-2 alone, or RUNX-2 and core-binding factor β (CBFβ). Bars show the mean and SD relative luciferase activity (ratio of firefly activity to *Renilla* activity) of 3 wells per group. TSS = transcription start site (see Figure 2 for other definitions).

We therefore prepared the 30-bp element (from −89 to −60 bp) containing the identified region for further analyses, and called it the hypertrophy box (HY box) (Figure 4). To determine the core responsive element in the HY box, we performed site-directed mutagenesis analysis of the luciferase assay by creating 3

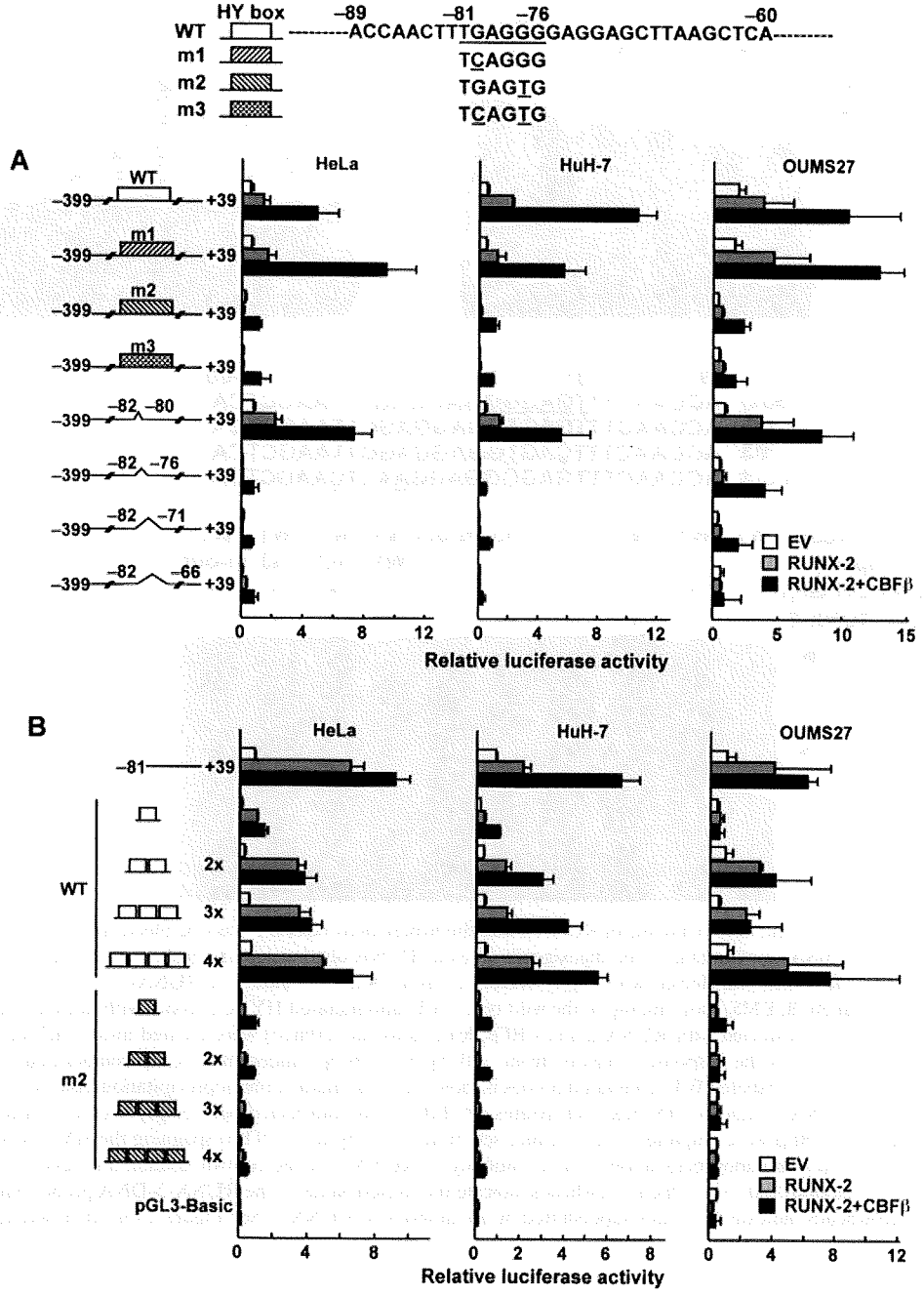


**Figure 4.** Luciferase assays for determination of the core responsive element in the hypertrophy box (HY box; −89 bp to −60 bp) containing the identified responsive region (from −81 bp to −76 bp, underlined) in the human COL10A1 promoter by site-directed mutagenesis (underlined) and deletion, and dose-response analysis of the tandem repeats using 3 human cell lines cotransfected with empty vector (control), RUNX-2 alone, or RUNX-2 and the coactivator core-binding factor β (CBFβ). **A,** Single-base mutations (m1 and m2), a double-base mutation (m3), and 1–15-bp deletions starting at the −81 bp site were created in the HY box of the 5′-end flanking region between −339 bp and +39 bp, and luciferase activity was compared with that in the wild-type (WT) HY box. **B,** Dose-response analysis of the tandem repeats of the WT and the mutated (m2) HY box was performed. Bars show the mean and SD relative luciferase activity of 3 wells per group. See Figure 2 for other definitions.

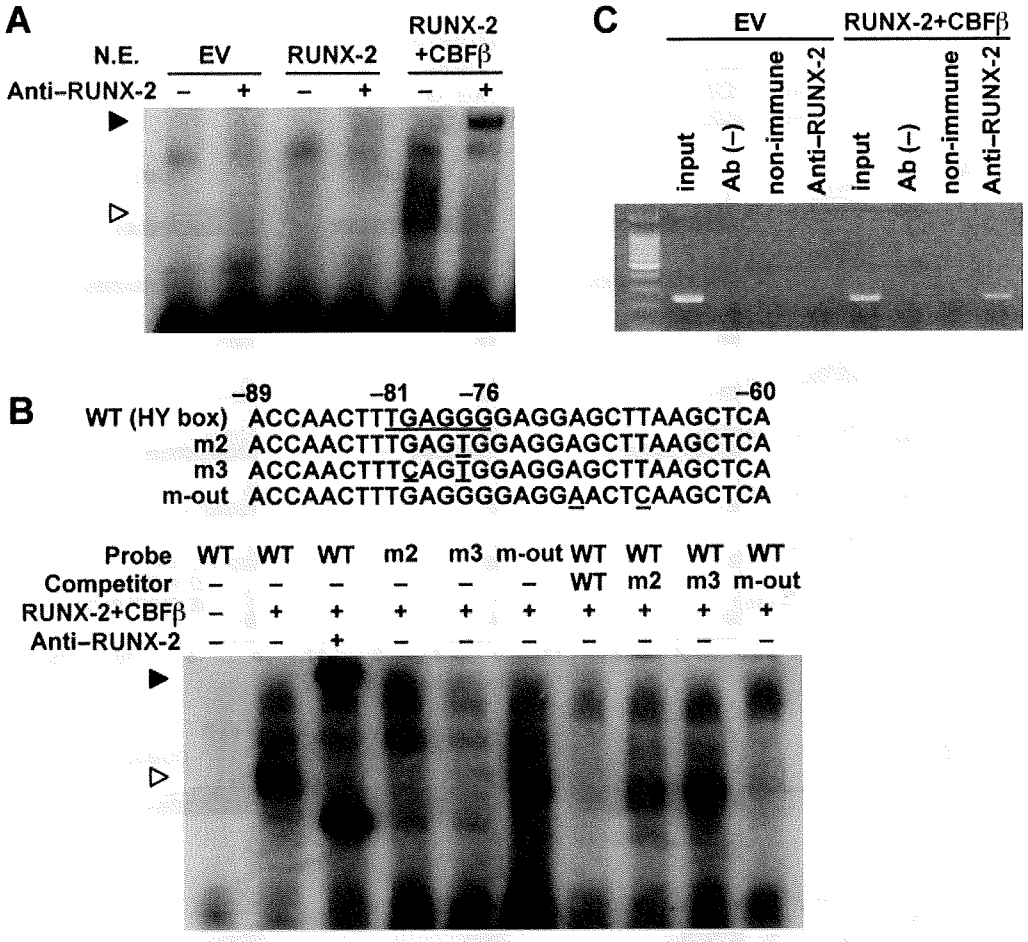


**Figure 5.** In vitro and in vivo binding of RUNX-2 and the hypertrophy box (HY box). **A,** Electrophoretic mobility shift assay (EMSA) for binding of the digoxigenin-labeled HY box oligonucleotide probe with nuclear extracts (N.E.) of COS-7 cells transfected with empty vector (control), RUNX-2 alone, or RUNX-2 and core-binding factor β (CBFβ). **B,** EMSA for binding of the wild-type (WT) and mutated HY box probes with nuclear extracts of COS-7 cells transfected with RUNX-2 and CBFβ. Mutations (underlined) were created inside (m2 and m3) and outside (m-out) the responsive region (from −81 bp to −76 bp; underlined). Cold competition with a 100-fold excess of unlabeled WT or mutated probes is shown. **C,** Chromatin immunoprecipitation assay for in vivo binding of RUNX-2 and the HY box. Cell lysates of HuH7 cells transfected with empty vector (control) or RUNX-2 and CBFβ were amplified with a primer set (from −113 bp to +119 bp) spanning the HY box before (input) and after immunoprecipitation with an antibody to RUNX-2 or the control nonimmune IgG or in the absence of antibody (Ab [−]). Open arrowheads indicate the shifted bands of the RUNX-2–DNA probe complex; solid arrowheads indicate the bands supershifted by an antibody to RUNX-2. See Figure 2 for other definitions.

mutations in the identified responsive region (mutation 1 at −80 bp, mutation 2 at −77 bp, and mutation 3 at both −80 bp and −77 bp) of the fragment between −339 bp and +39 bp (Figure 4A). Transactivation by RUNX-2 alone and in combination with CBFβ was suppressed by mutation 2 and mutation 3, but not by mutation 1, indicating that the −77 bp site is crucial for the transactivation of COL10A1 by RUNX-2. Luciferase assays by 1–15-bp deletions starting at the −81 bp site in the HY box confirmed that promoter activation by RUNX-2 was suppressed when the −77 bp site was included in the deletions (Figure 4A). Dose-response analysis of tandem repeats of the wild-type and the mutated (mutation 2) HY box clearly revealed that the wild-type HY box responded to RUNX-2 alone and in combination with CBFβ in a repeat number–dependent manner in all cells, while mutation 2 at the −77 bp site markedly suppressed the responses (Figure 4B).

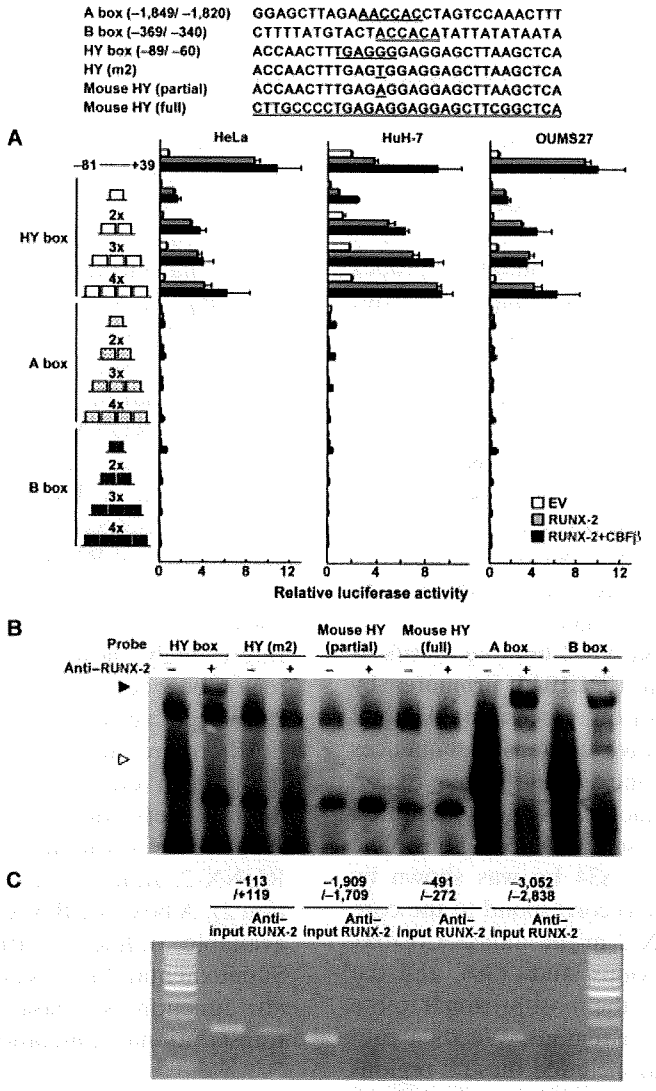


**Figure 6.** RUNX-2 transactivation of and binding to the A box (from –1849 bp to –1820 bp), B box (from –369 bp to –340 bp), and HY box (from –89 bp to –60 bp) in the human COL10A1 promoter. **A,** Response of luciferase activity to tandem repeats of the HY box, A box, and B box using human cells cotransfected with empty vector (control), RUNX-2 alone, or RUNX-2 and core-binding factor β (CBFβ). Bars show the mean and SD relative luciferase activity of 3 wells per group. **B,** Electrophoretic mobility shift assay (EMSA) for specific binding of digoxigenin-labeled oligonucleotide probes of the HY box, A box, and B box with nuclear extracts of COS-7 cells transfected with RUNX-2 and CBFβ. In addition to the 3 human elements, binding of 3 mutated HY box probes (m2) that mutated to the corresponding mouse sequence only at −77 bp in the core responsive region (mouse HY [partial]), and that fully mutated to the corresponding mouse sequence (mouse HY [full]) were examined. Open arrowheads indicate shifted bands of the RUNX-2–DNA complex; solid arrowheads indicate bands supershifted by an antibody to RUNX-2. **C,** Chromatin immunoprecipitation assay for in vivo binding of RUNX-2 with the human elements. Cell lysates of HuH7 cells transfected with RUNX-2 and CBFβ were amplified with a primer set spanning the HY box (from –113 bp to +119 bp), A box (from –1,909 bp to –1,709 bp), or B box (from –491 bp to –272 bp), or a primer set that did not include a RUNX-2 binding motif (from –3,052 bp to –2,838 bp) before (input) and after immunoprecipitation with an antibody to RUNX-2.

**Specific binding of RUNX-2 to the HY box.** We further examined in vitro and in vivo binding of RUNX-2 to the HY box by EMSA and ChIP assay, respectively. EMSA showed complex formation by the HY box oligonucleotide probe and nuclear extracts of COS-7 cells transfected with RUNX-2 and CBFβ (Figure 5A). The complex was barely detected with nuclear extracts of cells transfected with RUNX-2 alone, suggesting that CBFβ is necessary for binding. However, supershift of the complex by an antibody to RUNX-2